

Article

Iron(III) Complexes with Substituted Salicylaldehydes: Synthesis, Interaction with DNA and Serum Albumins, and Antioxidant Activity

Zisis Papadopoulos , Antonios G. Hatzidimitriou  and George Psomas * 

Laboratory of Inorganic Chemistry, Department of Chemistry, Aristotle University of Thessaloniki, GR-54124 Thessaloniki, Greece

* Correspondence: gepsomas@chem.auth.gr

Abstract: Metal complexes of endogenous metals, such as iron, copper, and zinc, offer a biocompatible, cost-effective, and eco-friendly alternative to heavy metals for drug design. This study presents the synthesis, structural characterization, and evaluation of the biological activity of eight novel iron(III) complexes with substituted salicylaldehydes as ligands. The characterization of the complexes involved spectroscopic and physicochemical methods. The structures of two complexes were determined using single-crystal X-ray crystallography. The biological studies of the complexes focused on the interaction of calf-thymus DNA, the (photo)cleavage of pBR322 plasmid DNA (pDNA), the affinity for bovine and human serum albumins, and the antioxidant activity. The complexes interacted with calf-thymus DNA via intercalation with high DNA-binding constants. The complexes exhibited high pDNA-cleavage ability, which is significantly enhanced upon exposure to UVA or UVB irradiation. The complexes can bind tightly and reversibly to both serum albumins, and their binding locations were identified. Finally, the complexes showed moderate ability to scavenge 1,1-diphenyl-picrylhydrazyl and 2,2'-azinobis-(3-ethylbenzothiazoline-6-sulfonic acid) radicals with a high ability to reduce hydrogen peroxide.

Keywords: iron(III) complexes; substituted salicylaldehydes; interaction with DNA; cleavage of plasmid DNA; affinity for albumins; antioxidant activity



Academic Editors: Fernando Mendes, Adenilson Oliveira dos Santos and Francisco Ferreira De Sousa

Received: 7 May 2025

Revised: 23 May 2025

Accepted: 27 May 2025

Published: 29 May 2025

Citation: Papadopoulos, Z.; Hatzidimitriou, A.G.; Psomas, G. Iron(III) Complexes with Substituted Salicylaldehydes: Synthesis, Interaction with DNA and Serum Albumins, and Antioxidant Activity. *Molecules* **2025**, *30*, 2383. <https://doi.org/10.3390/molecules30112383>

Copyright: © 2025 by the authors. Licensee MDPI, Basel, Switzerland. This article is an open access article distributed under the terms and conditions of the Creative Commons Attribution (CC BY) license (<https://creativecommons.org/licenses/by/4.0/>).

1. Introduction

There are over eight thousand rare diseases worldwide, affecting the lives of over 350 million people. Remarkably, there are approved therapies for only 5% of them [1,2]. Furthermore, drug resistance renders many previously effective drugs inactive, increasing the need for new drugs. Metal complexes are in the spotlight because of their advantages (their variety in structure, different charge possibilities, redox activity, luminescence, magnetic properties, etc.) compared to conventional organic drugs. Until today, there have been many metal complexes that are widely used in therapy and diagnosis, such as cisplatin and other platinum drugs, as well as gadolinium and technetium-99 m complexes [3,4].

The selection of iron complexes over other metals is based on several factors that may lead to a reduction in side-effects caused by platinum drugs. Iron is an endogenous element (the most abundant transition metal) in the human body, and its biological significance has been known since antiquity [5]. Because of its ability to interconvert between oxidation states +2 and +3, iron is crucial for important biological functions, including the transportation of oxygen and electrons, cellular metabolism, respiration, DNA synthesis [6,7], and photosynthesis [8]. Despite its beneficial effects, disorders on iron homeostasis may

result in iron deficiency or an iron overload, leading to heart failure [9], brain aging, and neurodegenerative diseases (such as Alzheimer's disease and Parkinson's disease), and its excess may result in free radical chain reactions causing tissue damages [10] or even tumors and other cancers [11,12]. It is believed that metal complexes of endogenous metals could have reduced side-effects compared to heavy metals because there is a well-regulated system of uptake, administration, and excretion in organisms. Additionally, such metal complexes suggest economically and environmentally sound options, potentially leading to cost-effective drug production [13]. Within this context, bioinorganic chemists are studying the potential activity of iron compounds, including reports regarding the antimicrobial and cytotoxic activity of iron oxide nanoparticles [14,15], as well as the anticancer [16], antimicrobial [17–19], and antioxidant [19–22] efficacy of iron complexes.

Substituted salicylaldehydes (X-saloH, Figure 1) are produced from salicylaldehyde (2-hydroxy-benzaldehyde, saloH, Figure 1), which is a natural product found in many metabolic procedures such as metabolites, intermediates, or defensive chemicals [23]. Many of the existing X-saloH compounds exhibit interesting antimicrobial and antioxidant activity, depending on the nature of the substituents [24–26]. This interesting biological profile, along with their ability to form stable complexes through strong bidentate coordination via the aldehyde and phenolato-oxygen atoms, has triggered many studies over the past few years. Within this context, different metal ions (such as Mn(II), Fe(III), Co(II), Ni(II), Cu(II), Zn(II), Ru(II), Pd(II), Cd(II), Mo(VI)O₂, Re(V)O, and Er(III)) have been used for the preparation of complexes with substituted salicylaldehydes [27–48]. Although the biological properties of most of those complexes have been studied, there are not many reports on the biological activity of iron complexes with this family of ligands [49,50].

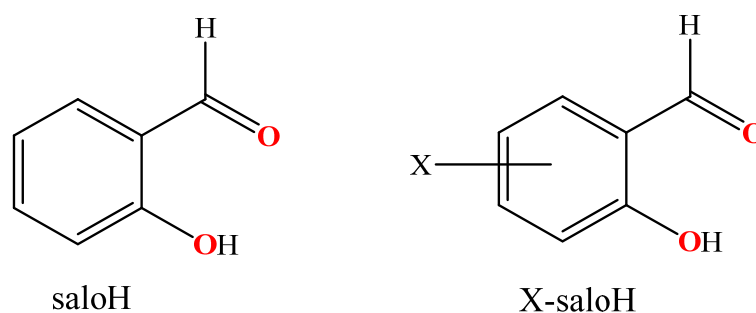


Figure 1. The syntax formula for salicylaldehyde (saloH) and substituted salicylaldehyde (X-saloH).

In the context of our continuous research regarding the synthesis, characterization and biological evaluation of metal complexes with substituted salicylaldehydes [27–40], the commercially available substituted salicylaldehydes 2-hydroxy-1-naphthaldehyde (1naph-saloH), 3-methoxy-salicylaldehyde (*o*-vanillin, ovanH), 5-methyl-salicylaldehyde (5Me-saloH), 3-ethoxy-salicylaldehyde (3EtO-saloH), 4-hydroxy-salicylaldehyde (4OH-saloH), 4-methoxy-salicylaldehyde (4MeO-saloH), 4-diethylamino-salicylaldehyde (4Et₂N-saloH), and 3,5-dibromo-salicylaldehyde (3,5diBr-saloH) were employed for the synthesis of iron(III) complexes (Figure 2). The reaction of these deprotonated X-salo[−] compounds with Fe(III) yielded eight novel neutral iron(III) complexes, namely [Fe(1naph-salo)₃] (**1**), {K[Fe(ovan)₃]₂}Cl·CH₃OH (**2**), [Fe(5Me-salo)₃] (**3**), [Fe(3EtO-salo)₃] (**4**), [Fe(4OH-salo)₃] (**5**), [Fe(4MeO-salo)₃] (**6**), [Fe(4Et₂N-salo)₃] (**7**), and [Fe(3,5-diBr-salo)₃] (**8**), respectively, which were characterized with spectroscopic (IR and UV-vis spectroscopies) and physicochemical techniques. In particular, the crystal structures of complexes **1** and **2** were determined using single-crystal X-ray crystallography.

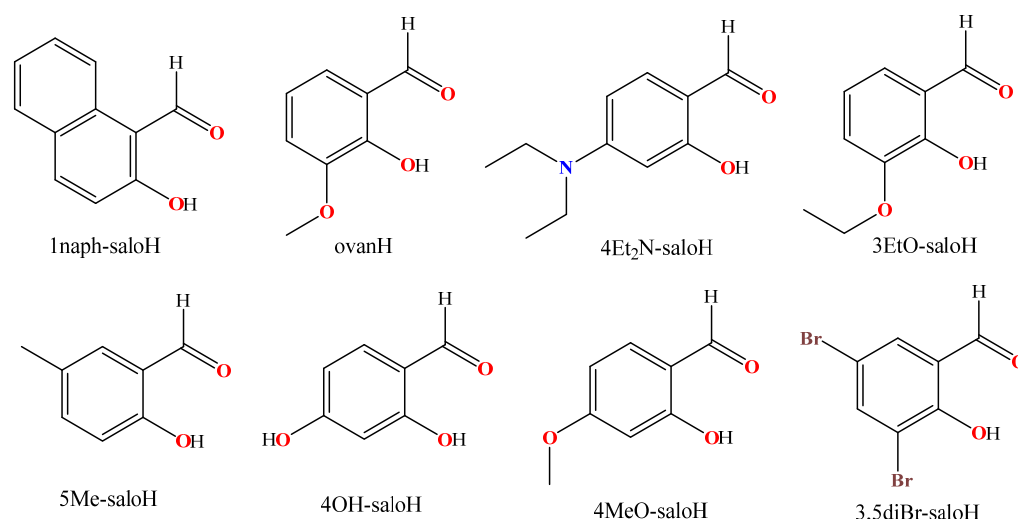


Figure 2. The syntax formulae of the substituted salicylaldehydes used herein (1naph-saloH = 2-hydroxy-1-naphthaldehyde; ovan = 3-methoxy-salicylaldehyde = *o*-vanillin; 4Et₂N-saloH = 4-diethylamino-salicylaldehyde; 3EtO-saloH = 3-ethoxy-salicylaldehyde; 5Me-saloH = 5-methyl-salicylaldehyde; 4OH-saloH = 4-hydroxy-salicylaldehyde; 4MeO-saloH = 4-methoxy-salicylaldehyde; 3,5diBr-saloH = 3,5-dibromo-salicylaldehyde).

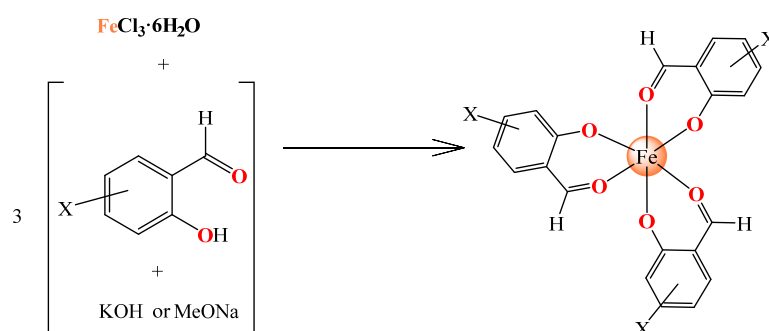
Regarding the biological activity of complexes **1–8**, we focused on their interaction with DNA and serum albumins, as well as their antioxidant activity. As for the interaction of complexes **1–8** with calf-thymus (CT) DNA, the calculation of the corresponding binding constants (K_b) and thermodynamic parameters (ΔH , ΔS , and ΔG) in response to changes in temperature, the assessment of the DNA-interaction mode, and the competition with ethidium bromide (EB) were achieved via the combination of viscosity measurements, and UV-vis and fluorescence emission spectroscopies. The efficacy of complexes **1–8** in cleaving supercoiled circular pBR322 plasmid DNA (pDNA) and the effect of UVA, UVB, or visible light on this ability were evaluated using agarose gel electrophoresis. Additionally, the binding affinity and albumin-binding location of complexes **1–8** with bovine (BSA) and human serum albumins (HSAs) were monitored with fluorescence emission spectroscopy. Finally, the antioxidant activity of complexes **1–8** was assessed by examining the ability to scavenge 1,1-diphenyl-picrylhydrazyl (DPPH) and 2,2'-azino-bis-(3-ethylbenzothiazoline-6-sulfonic acid) (ABTS) free radicals and their behavior towards H₂O₂.

2. Results

2.1. Synthesis and Characterization

In order to obtain complexes **1–8**, the substituted salicylaldehydes, after being in situ deprotonated on the phenolic hydroxyl group with a strong base (CH₃ONa or KOH), were added in a methanolic solution of FeCl₃·6H₂O. This reaction efficiently yielded the final neutral homoleptic Fe(III) complexes (Scheme 1). The characterization of the complexes was achieved through physicochemical and spectroscopic techniques (IR and UV-vis) and, especially for complexes **1** and **2**, single-crystal X-ray crystallography.

All complexes were soluble in DMSO and DMF, partially soluble in methanol, and insoluble in most organic solvents and H₂O. The molar conductivity of the complexes was measured in a 1 mM DMSO solution, and the Λ_M values were in the range of 10–16 mho·cm²·mol⁻¹, indicating that the complexes were non-electrolytes in solution [51] bearing a 1:3 Fe(III):(X-salo) composition. These data were confirmed from elemental analysis data and were in good agreement with the suggested molecular formulae.



Scheme 1. The synthetic procedure for complexes 1–8.

The changes observed in the IR spectra of complexes 1–8 (Figure S1), when compared to the spectra of the free salicylaldehydes, confirmed the deprotonated and the bidentate coordination of the X-salo ligands. In the spectra of free X-saloH, the stretching vibration attributed to aldehyde C=O, $\nu(\text{C}=\text{O})$, was found in the range of $1621\text{--}1663\text{ cm}^{-1}$. In the spectra of the complexes, a shift in the corresponding $\nu(\text{C}=\text{O})$ towards lower values (in the range of $1600\text{--}1626\text{ cm}^{-1}$ with $\Delta\nu = 6\text{--}58\text{ cm}^{-1}$) was observed, revealing the weakening of the C=O bond as a result of the coordination of the aldehyde oxygen atoms to Fe(III) ion [28–30,39]. In addition, the band assigned to the stretching vibration of the phenolic C–O bond, $\nu(\text{C}–\text{O})$, observed at $1272\text{--}1293\text{ cm}^{-1}$ in the spectra of free X-saloH, exhibited a positive shift in $\Delta\nu = 27\text{--}44\text{ cm}^{-1}$ upon coordination to higher wavenumbers (in the range $1306\text{--}1324\text{ cm}^{-1}$) revealing the coordination of the phenolato-oxygen atoms to Fe(III) ion [28–30,39]. In conclusion, in all complexes 1–8, the substituted salicylaldehyde ligands were coordinated to Fe(III) ions in a bidentate chelating mode through the phenolato- and aldehyde oxygens.

The electronic spectra of the complexes were measured in a DMSO solution and in a solid state. The spectra were similar, suggesting that the complexes retained their structure in solution. In the visible region of the spectrum, a band located at $\lambda_{\text{max}} = 460\text{--}501\text{ nm}$ ($\epsilon = 190\text{--}600\text{ M}^{-1}\text{ cm}^{-1}$) was observed for most complexes which may be assigned to a d–d (${}^6\text{A}_{1g} \rightarrow {}^5\text{T}_{1g}$ or ${}^6\text{A}_{1g} \rightarrow \text{T}_{2g}(\text{G})$) transition [21,22,52]; however, in some cases, this band overlapped from the neighboring band located in the range $400\text{--}427\text{ nm}$ attributed to metal-to-ligand charge-transfer transitions, which is characteristic for distorted octahedral Fe^{3+} complexes with salicylaldehydes and hydroxyphenones [42,53]. In addition, the bands observed in the UV region of the spectra are attributed to intraligand transitions.

2.2. Structures the Complexes

Among the eight novel $[\text{Fe}(\text{X-salo})_3]$ complexes studied herein, single-crystals suitable for X-ray crystallography structural determination were obtained only for complexes 1 and 2. The experimental X-ray crystallography details for these complexes are summarized in Table S1. The structural characterization of complexes 3–8 was performed based on derived experimental data in comparison with existing structures.

2.2.1. Crystal Structures of Complexes 1 and 2

Complex 1 was crystallized in the monoclinic crystal system and C2/c space group (Table S1). The molecular structure of complex 1 is shown in Figure 3, and selected bond lengths and angles are summarized in Table S2. Complex 1 is a mononuclear iron(III) complex consisting of three deprotonated 1naph-salo[−] ligands (Figure 3). The 1naph-salo[−] ligands are coordinated to iron(III) ions in a bidentate chelating mode through their carbonyl oxygen (O1, O3, and O5) and their phenolato (O2, O4, and O6)-oxygen atoms with Fe1–O bond distances in the range $1.965(3)\text{--}2.042(3)\text{ \AA}$ (Table 1). Such bidentate coordination is typical for the 1naph-salo[−] ligands reported in the structures of diverse

metal complexes [54–56]. The largest angles in the coordination sphere of Fe(III) are in the range 169.30(14)–175.24(13)° (Table S2), indicating a distorted octahedral geometry.

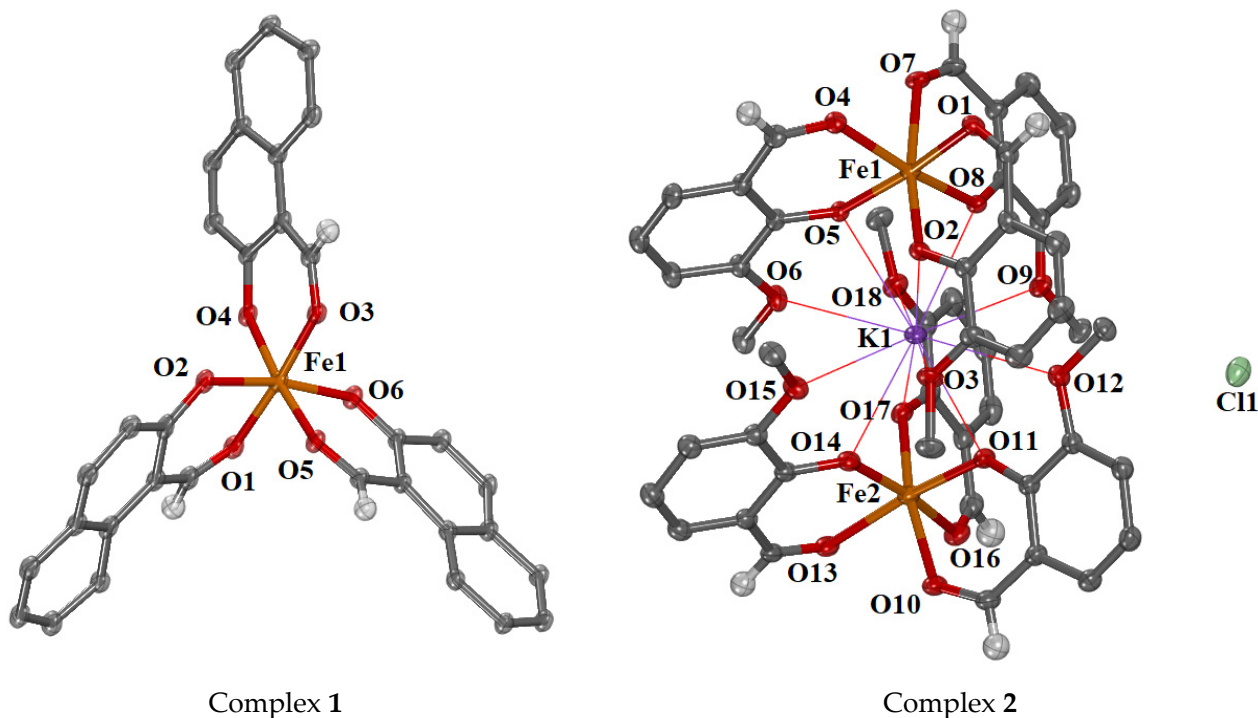


Figure 3. Crystal structures of complexes 1 and 2. In complex 2, the interactions of the hosted potassium cation (K1) with the oxygen atoms are given in thin lines. Aromatic hydrogen atoms with methanol solvate molecules and low-occupation counter anions are omitted for clarity.

Table 1. Selected lengths of bonds (in Å) for complexes 1 and 2.

| Bond | Length (Å) | Bond | Length (Å) |
|---------------------------------|------------|-----------------------------------|------------|
| Complex 1 | | | |
| Fe–O _{aldehyde} | | Fe–O _{phenolato} | |
| Fe1–O1 | 1.976(4) | Fe1–O2 | 2.024(3) |
| Fe1–O3 | 1.994(4) | Fe1–O4 | 1.965(3) |
| Fe1–O5 | 2.042(3) | Fe1–O6 | 1.967(3) |
| Complex 2 | | | |
| Fe–O _{aldehyde} | | Fe–O _{phenolato} | |
| Fe1–O1 | 2.0673(18) | Fe1–O2 | 1.9344(16) |
| Fe1–O4 | 2.0656(18) | Fe1–O5 | 1.9357(16) |
| Fe1–O7 | 2.0755(17) | Fe1–O8 | 1.9384(17) |
| Fe2–O10 | 2.049(2) | Fe2–O11 | 1.9346(19) |
| Fe2–O13 | 2.070(2) | Fe2–O14 | 1.933(2) |
| Fe2–O16 | 2.080(2) | Fe2–O17 | 1.942(2) |
| K \cdots O _{methoxy} | | K \cdots O _{phenolato} | |
| K1 \cdots O3 | 3.101(2) | K1 \cdots O2 | 2.9761(18) |
| K1 \cdots O6 | 3.078(2) | K1 \cdots O5 | 2.9155(17) |
| K1 \cdots O9 | 3.054(2) | K1 \cdots O8 | 2.8843(17) |
| K1 \cdots O12 | 3.097(2) | K1 \cdots O11 | 2.8776(19) |
| K1 \cdots O15 | 3.136(2) | K1 \cdots O14 | 2.8616(19) |
| K1 \cdots O18 | 3.227(2) | K1 \cdots O17 | 2.998(2) |

Complex **2** crystallized in the triclinic crystal system and $P\bar{1}$ space group. The molecular structure of complex **2** is depicted in Figure 3, and selected bond lengths and angles are summarized in Table S3. The asymmetric unit of the complex contains two crystallographically independent mononuclear Fe(III) moieties of the formula $[\text{Fe}(\text{ovan})_3]$, a potassium ion, a chlorido ion (disordered over two positions), and a methanol solvate molecule (disordered over two positions).

In each mononuclear iron(III) moiety, the deprotonated ovan^- ligands are coordinated to Fe(III) ion bidentately through their aldehyde and phenolato-oxygen atoms as previously reported for this type of complex [36,57–59]. The $\text{Fe}-\text{O}_{\text{phenolato}}$ bond distances are in the range 1.933(2)–1.9384(17) Å and are shorter than the $\text{Fe}-\text{O}_{\text{aldehyde}}$ bond distances (2.049(2)–2.0755(17) Å). Regarding the structures of iron complexes with *o*-vanillin, two reports were found in the literature [58,59], the mononuclear iron(III) complexes $[\text{Fe}(\text{ovan})_2(\text{H}_2\text{O})_2]$ [58] and $[\text{Fe}(\text{ovan})_2(\text{H}_2\text{O})\text{Cl}]$ [59] which contained two ovan^- ligands and the methoxy oxygen did not participate in any kind of binding. Therefore, complex **2** is the first iron complex with a 1:3 Fe:(ovan^-) ratio. The largest angles in the Fe1 and Fe2 coordination spheres are in the range 166.06(8)–170.14(7)° (Table S3), suggesting a distorted octahedral geometry around each Fe(III) ion. In both Fe(III) moieties, the corresponding oxygen atoms lie at *cis* positions to each other ($\text{O}_{\text{phenolato}}-\text{Fe1}/2-\text{O}_{\text{phenolato}} = 90.59(7)-90.23(9)^\circ$; $\text{O}_{\text{aldehyde}}-\text{Fe1}/2-\text{O}_{\text{aldehyde}} = 82.98(7)-84.38(8)^\circ$).

The relative arrangement of the two $[\text{Fe}(\text{ovan})_3]$ in the lattice is such that it enables the encapsulation of a potassium ion in the interstitial space. K1 interacts electrostatically with the phenolato (O2, O5, O8, O11, O14, and O17) and methoxy (O3, O6, O9, O12, O15, and O18) oxygen atoms of the six surrounding ovan^- ligands at distances of 2.8616(19)–2.998(2) Å (for $\text{K1}\cdots\text{O}_{\text{phenolato}}$) and 3.054(2)–3.227(2) Å (for $\text{K}\cdots\text{O}_{\text{methoxy}}$), respectively (Table 1). The methoxy oxygen atoms of ovan^- ligands may participate in the coordination mainly in polynuclear complexes where *o*-vanillin acts as the bridging ligand [60–65]. The positive charge in K1 is neutralized by a chlorido anion found in the asymmetric unit.

In the literature, there are reports concerning diverse complexes hosting potassium ions. [66–68]. More specifically, in complex $\{[\text{Ni}(\text{hab})]\text{K}[\text{habNi}]\}\cdot\text{SCN}$ (where H_2hab is bis(2-hydroxy-3-methoxybenzylidene)-1,2-diaminobenzene, an *o*-vanillin derivative), the $\text{K}\cdots\text{O}$ distances are in the range 2.596 Å–2.725 Å [68]. In reported complexes and crown ethers hosting potassium ions, the $\text{K}\cdots\text{O}$ distances were found in the range 2.67–2.88 Å [66,67,69–71]. In complex **2**, the $\text{K}\cdots\text{O}$ distances are longer and may be considered interaction distances rather than classified as weak electrostatic or supramolecular contacts.

2.2.2. Proposed Structures for Complexes 3–8

The structures of complexes **3–8** may be proposed based on the experimental data collected from elemental analysis, molar conductivity measurements, and infrared and electronic spectroscopies. In these compounds with the general formula $[\text{Fe}(\text{X-salo})_3]$, the deprotonated X-salo^- ligands are bound to Fe(III) ions in a bidentate fashion through the aldehyde and phenolato-oxygen atoms. In complexes **3–8** (Scheme 1, Figure S2), the Fe(III) ions are six-coordinated with an FeO_6 coordination sphere adopting distorted octahedral geometry similar to that found for complex **1**.

2.3. Interaction of the Complexes with CT DNA

It is important to study the binding affinity of the compounds with DNA as an initial approach for further biomedical applications. The interaction of metal complexes with DNA takes place via covalent bonding or the development of non-covalent forces (leading to intercalation, electrostatic interactions, and groove-binding) or may induce the cleavage

of the DNA double helix [72,73]. As a means to shed light on the nature of the interaction of complexes 1–8 with CT DNA, UV-vis spectroscopy, DNA viscosity measurements, and EB displacement studies were employed.

2.3.1. Interaction of the Complexes with CT DNA Studied with UV-Vis Spectroscopy

UV-vis spectroscopy titrations were used to initially evaluate the interaction of complexes 1–8 with CT DNA. For this purpose, the UV-vis spectra of the complexes and the changes in the observed bands were monitored in the presence of incrementally increased amounts of CT DNA (Figure S3). Most of these bands showed a slight hypochromism, which was often accompanied by a bathochromic shift (Table 2). In some cases, a hyperchromic shift in the bands was also recorded. These features confirmed the interaction of the complexes with CT DNA, forming a new DNA-complex adduct and leading to a stabilized system [74]. These findings provide initial evidence of the interaction between the complexes and CT DNA. However, it is not safe to suggest a DNA-interaction mode, and for this reason, more studies are necessary.

Table 2. UV-vis spectroscopic data for the interaction of complexes 1–8 with CT DNA: UV-band (λ_{\max} , in nm) (percentage of the observed hyper-/hypo-chromism ($\Delta A/A_0$, in %) and blue/red shift in the λ_{\max} ($\Delta\lambda$, in nm)); DNA-binding constant (K_b , in M^{-1}).

| Compound | λ_{\max} (nm) ($\Delta A/A_0$ (%) ^a , $\Delta\lambda$ (nm) ^b) | K_b (M^{-1}) |
|---|--|------------------------------|
| [Fe(1naph-salo) ₃], 1 | 315(−23 ^a , −9 ^b); 356(<− ^c , +7); 408(>+ ^d , +1) | $1.62(\pm 0.01) \times 10^7$ |
| {K[Fe(ovan) ₃] ₂ }Cl, 2 | 320(−14, +13); 354(−10, +1); 410(>+, +1) | $1.65(\pm 0.13) \times 10^6$ |
| [Fe(5Me-salo) ₃], 3 | 333(−35, +5); 409(>+, +3) | $9.12(\pm 0.95) \times 10^5$ |
| [Fe(3EtO-salo) ₃], 4 | 340(−24, 0); 379(>+, −5) | $8.89(\pm 0.14) \times 10^4$ |
| [Fe(4OH-salo) ₃], 5 | 278(<−, −4); 315(>+, +15) | $6.64(\pm 1.06) \times 10^5$ |
| [Fe(4MeO-salo) ₃], 6 | 282(−17, −9); 316(<−, +2); 386(>+, −2.5) | $6.17(\pm 1.13) \times 10^5$ |
| [Fe(4Et ₂ N-salo) ₃], 7 | 349(+12, −1); 407(<−, 0) | $5.62(\pm 1.09) \times 10^5$ |
| [Fe(3,5diBr-salo) ₃], 8 | 319(−30, +3); 426(>+, 0) | $1.05(\pm 0.21) \times 10^6$ |
| 1naph-saloH | 315(−22, −9); 356(−62, +9); 409(>+, +2) | $1.97(\pm 0.10) \times 10^6$ |
| ovanH [37] | 340(−28, +3); 400(sh) ^e (+, 0) | $9.84(\pm 0.16) \times 10^4$ |
| 5Me-saloH [37] | 335(−10, 0) | $1.17(\pm 0.11) \times 10^6$ |
| 3EtO-saloH | 267(−25, 0); 340(−33, +4); 403(>+, +4) | $1.16(\pm 0.13) \times 10^6$ |
| 4OH-saloH | 282(−13, −1); 315(+24, +21) | $2.38(\pm 0.17) \times 10^5$ |
| 4MeO-saloH [27] | 315(−44, +1) | $9.25(\pm 0.12) \times 10^5$ |
| 4Et ₂ N-saloH [30] | 349(−1, 0) | $5.06(\pm 0.14) \times 10^5$ |
| 3,5diBr-saloH [39] | 337(<−, elim ^f); 427(>+, 0) | $3.71(\pm 0.14) \times 10^5$ |

^a “+” denotes hyperchromism; “−” denotes hypochromism. ^b “+” denotes red shift; “−” denotes blue shift. ^c “<−” denotes intense hypochromism. ^d “>+” denotes intense hyperchromism. ^e “(sh)” = (shoulder). ^f “elim” = eliminated.

The DNA-binding constants (K_b) of the complexes were calculated with the Wolfe-Shimer equation (Equation (S1)) [75] and the plots of $[DNA]/(\epsilon_A - \epsilon_f)$ versus $[DNA]$ (Figure S4). Most complexes 1–8 had higher K_b values than the corresponding free X-saloH; the K_b values were in the range $8.89(\pm 0.14) \times 10^4 - 1.62(\pm 0.01) \times 10^7 M^{-1}$, showing tight interactions with CT DNA (Table 2). Complex 1 exhibited the highest K_b value ($1.62(\pm 0.01) \times 10^7 M^{-1}$, Table 2) among the compounds studied herein, which was probably due to the extended aromatic system of the 1naph-salo[−] ligand. Apart from complex 4, the K_b values of all complexes 1–8 were higher than that of the classical intercalator EB ($K_b = 1.23 \times 10^5 M^{-1}$) [76]. Compared to previously reported metal complexes with substituted salicylaldehydes [27–40], the synthesized complexes exhibited similar or higher K_b values and were ranked as the tightest DNA binder among the metal-(X-salo) complexes.

2.3.2. CT DNA Viscosity Measurements

DNA viscosity measurements were performed in order to clarify the interaction mode of the complexes with DNA. Such measurements are useful since the changes in relative DNA viscosity are proportional to changes in relative DNA length. An increase in DNA viscosity is observed in the presence of classic intercalative agents whose insertion in between DNA bases increases the overall DNA-length. On the other hand, in the case of the nonclassical intercalator (i.e., including groove binders or compounds such as electrostatic interactions), practically stable or slightly decreased DNA viscosity is observed [77]. In the case of complexes 1–8, the viscosity of a CT DNA solution (0.1 mM) was measured in the presence of incrementally increasing concentrations of each complex (Figure 4). For all the complexes, an increase in viscosity was noticed, which suggests an intercalative mode of interaction.

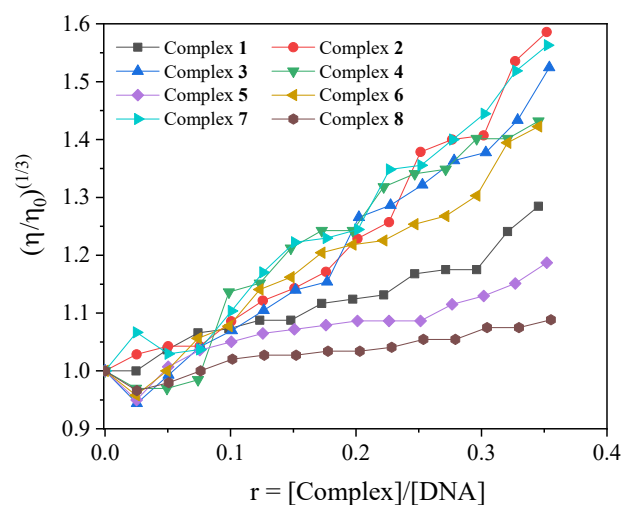


Figure 4. Relative viscosity $(\eta/\eta_0)^{1/3}$ of CT DNA (0.1 mM) in buffer solution (150 mM NaCl and 15 mM trisodium citrate at pH 7.0) in the presence of complexes 1–8 at increasing amounts ($r = [\text{compound}]/[\text{DNA}]$).

2.3.3. Competitive Studies with EB

EB is a DNA-intercalation marker since its intercalation to DNA, which occurs via the insertion of its planar phenanthridine ring in between two adjacent DNA bases, is evident from an intense fluorescence emission band at $\lambda_{\text{max}} = 592\text{--}594$ nm upon excitation at 540 nm [78]. The quenching of this band's intensity induced by the presence of the complexes will indicate their competition for the same DNA intercalation sites [78]. Therefore, a buffer solution of EB (40 μM) and CT DNA (40 μM) was pretreated for 1 h, and its fluorescence emission spectra were recorded (with $\lambda_{\text{excitation}} = 540$ nm) in the presence of incrementally increasing concentrations of each complex (Figure S5). An intense quenching of the EB-DNA emission band at $\lambda_{\text{max}} = 593$ nm was observed for all complexes (up to 79.1% of the initial fluorescence recorded for complex 8, Figure 5, Table 3).

The Stern-Volmer constants (K_{SV}) were calculated with the Stern-Volmer equation (Equation (S2)) [78] and the corresponding plots (Figure S6). All complexes presented relatively high K_{SV} values (Table 3), and complex 4 had the highest constant ($K_{\text{SV}} = 1.35(\pm 0.02) \times 10^5 \text{ M}^{-1}$). For the calculation of the quenching constants (K_{q}) for the complexes with Equation (S3), the value of 23 ns was applied as the fluorescence lifetime for the EB-DNA system (τ_0) [79]. The K_{q} values of all complexes were significantly higher (by two orders of magnitude) than $10^{10} \text{ M}^{-1} \text{ s}^{-1}$. Such high K_{q} values are evidence of a static quenching mechanism, confirming the formation of a new DNA compound adduct as a result of the displacement of EB [78].

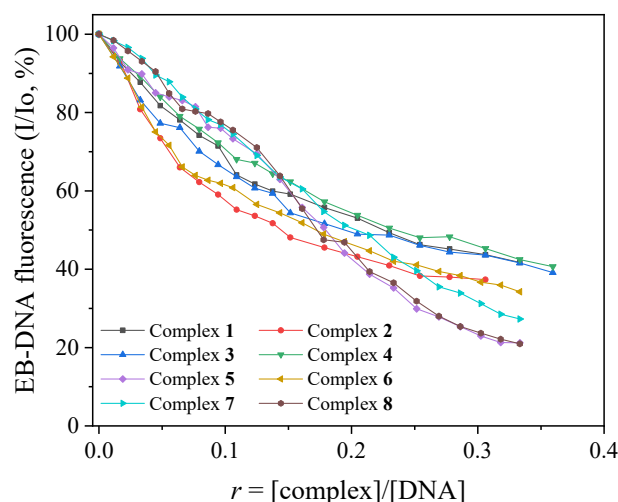


Figure 5. The plot of relative EB-DNA fluorescence emission intensity at $\lambda_{\text{emission}} = 593 \text{ nm}$ (I/I_0 , %) versus r ($r = [\text{complex}]/[\text{DNA}]$) in the presence of complexes 1–8 (up to 41.7% of the initial EB-DNA fluorescence for complex 1; 37.4% for complex 2; 39.1% for complex 3; 40.7% for complex 4; 21.2% for complex 5; 34.2% for complex 6; 27.3% for complex 7; and 20.9% for complex 8).

Table 3. Fluorescence features of the EB displacement studies for complexes 1–8: the percentage of EB-DNA fluorescence emission quenching ($\Delta I/I_0$, in %), Stern-Volmer (K_{SV} , in M^{-1}), and quenching constants (K_q , in $M^{-1} s^{-1}$).

| Compound | $\Delta I/I_0$ (%) | K_{SV} (M^{-1}) | K_q ($M^{-1} s^{-1}$) |
|---|--------------------|------------------------------|---------------------------------|
| [Fe(1naph-salo) ₃], 1 | 58.3 | $7.11(\pm 0.15) \times 10^4$ | $3.09(\pm 0.07) \times 10^{12}$ |
| {K[Fe(ovan) ₃] ₂ }Cl, 2 | 62.6 | $1.01(\pm 0.03) \times 10^5$ | $4.38(\pm 0.14) \times 10^{12}$ |
| [Fe(5Me-salo) ₃], 3 | 60.9 | $6.99(\pm 0.22) \times 10^4$ | $3.04(\pm 0.10) \times 10^{12}$ |
| [Fe(3EtO-salo) ₃], 4 | 59.3 | $1.35(\pm 0.02) \times 10^5$ | $5.88(\pm 0.08) \times 10^{12}$ |
| [Fe(4OH-salo) ₃], 5 | 78.8 | $8.58(\pm 0.35) \times 10^4$ | $3.73(\pm 0.15) \times 10^{12}$ |
| [Fe(4MeO-salo) ₃], 6 | 65.8 | $9.17(\pm 0.13) \times 10^4$ | $3.99(\pm 0.06) \times 10^{12}$ |
| [Fe(4Et ₂ N-salo) ₃], 7 | 72.7 | $1.17(\pm 0.06) \times 10^5$ | $5.08(\pm 0.25) \times 10^{12}$ |
| [Fe(3,5diBr-salo) ₃], 8 | 79.1 | $3.88(\pm 0.14) \times 10^4$ | $1.69(\pm 0.62) \times 10^{12}$ |

2.3.4. Thermodynamic Parameters for the Interaction of Complexes with CT DNA

The non-covalent forces developed between compounds and DNA are hydrophobic forces, electrostatic interactions, van der Waals interactions, and hydrogen bonds [80,81]. According to the literature, the signs of the values calculated for the changes in enthalpy (ΔH) and entropy (ΔS) may serve as evidence of the different interaction modes. More specifically, positive values of both ΔH and ΔS ($\Delta H > 0$ and $\Delta S > 0$) are indicative of the presence of hydrophobic forces, and negative values of both ΔH and ΔS ($\Delta H < 0$ and $\Delta S < 0$) are found upon the development of van der Waals interactions, while the combination of $\Delta H < 0$ and $\Delta S > 0$ is consistent with electrostatic interactions [81,82].

The K_b values of complexes 1–8 were determined for three different temperatures (298 K, 303 K, and 310 K). For all complexes 1–8, the increase in temperature resulted in higher K_b values (Table S4). The corresponding changes in enthalpy (ΔH) and entropy (ΔS) (Table S4) were calculated from the van't Hoff equation (Equation (S4)), and ΔG was obtained from the Gibb's-Helmholtz equation (Equation (S5)) and from the plots of $\ln(K_b)$ versus $(1/T)$ complexes 1–8 (where $-\Delta H/R$ is the slope and $\Delta S/R$ is the intercept of the fitting line while R is the universal gas constant, as shown in Figure S7). Both the values of ΔH and ΔS (Table S4) are positive, indicating that hydrophobic forces are developed between the complexes and CT DNA upon their interaction, i.e., π - π stacking interactions,

which are consistent with an intercalative interaction mode [83]. Furthermore, the negative ΔG values (Table S4) indicate a spontaneous interaction with CT DNA [81,83,84].

2.4. (Photo)Cleavage of pBR322 Plasmid DNA

The interaction of complexes 1–8 with plasmid DNA was studied in the presence and absence of irradiation. The complexes (500 μM) were incubated with pBR322 DNA in a tris buffer solution (25 μM , pH 6.8), ensuring that the final concentration of DMSO did not exceed 10% *v/v*. The effect of the compounds on pDNA was monitored after incubating the samples at 37 °C in the absence or presence of UV-B (irradiation at 312 nm for 30 min), UV-A (irradiation at 365 nm for 120 min), or visible light (irradiation for 120 min), and the results were analyzed with gel electrophoresis on 1% agarose stained with EB. The supercoiled pDNA appears as Form I in the gel after electrophoresis. The interaction of the compounds with pDNA may induce single-stranded (ss) or double-stranded (ds) damage, resulting in Form II (relaxed pDNA) and Form III (linear pDNA), respectively. In this case, the extent of pDNA damage is assessed by calculating the percentages of ss% and ds% with Equations (S6) and (S7) [85].

The reaction mixtures of pDNA and the compounds were incubated in the dark for 150 min and were then analyzed by 1% agarose gel electrophoresis with EB staining (Figure S8). In the absence of light, all complexes (500 μM) converted supercoiled pDNA into relaxed circular DNA (Form II) by inducing ss breaks with low-to-moderate percentages (up to 43% induced by complex 8).

The complexes proved to be more active when the mixture of pDNA compounds was exposed to radiation. When exposed to UVB radiation for 30 min, supercoiled pDNA was almost completely degraded due to the ss and ds breaks, and in some lanes, the smearing did not allow the respective percentages to be calculated (Figure S9). When exposed to UVA radiation for 120 min, the complexes were very active at inducing ss breaks to pDNA (Figure S10). In most cases, bands exhibiting delayed electrophoretic mobility compared to Form II of pDNA, which was observed and may be attributed to pDNA fragments of higher molecular weight [86,87]. Finally, the exposure to visible light resulted in the less pronounced activity of the complexes towards pDNA (Figure S11), causing ss and ds (of lower percentage) breaks.

In conclusion, exposure time and irradiation energy affected the photocleavage activity of the compounds. All the complexes became very active after exposure to UVA or UVB radiation at the concentration (of 500 μM) tested, showing their photoreactive potential.

2.5. Interaction of the Compounds with Albumins

Serum albumin (SA) is among the most abundant proteins of the circulatory system, with many biological roles, such as the regulation of normal blood volume and osmotic pressure and the reversible binding and transportation of drugs and other bioactive small molecules. Therefore, studying the interaction between albumins (either HSA or its structural analog BSA) with bioactive compounds may contribute to revealing altered new mechanistic pathways or differentiated biological properties of these compounds upon their interaction with SAs [78]. Within this context, the interaction of complexes 1–8 with BSA and HSA was studied with fluorescence emission spectroscopy.

The solutions of BSA and HSA exhibited an intense fluorescence emission band with $\lambda_{\text{em,max}}$ in the range of 340–350 nm, when excited at 295 nm [78] because of the tryptophan residues (Trp-134 and Trp-212 in BSA, and Trp-214 in HSA). The addition of complexes 1–8 into an SA solution (3 μM) resulted in a moderate-to-significant quenching of the albumin fluorescence emission bands (Figures S12 and S13). Complex 8 induced the highest quenching for both albumins (Figure 6). The observed quenching was assigned to

changes in the tryptophan environment of SA due to changes in its secondary structure resulting from the binding of the compounds to SA [78]. Furthermore, the influence of the inner-filter effect on the measurements was evaluated with Equation (S8) [88], but it was too low to affect the measurements.

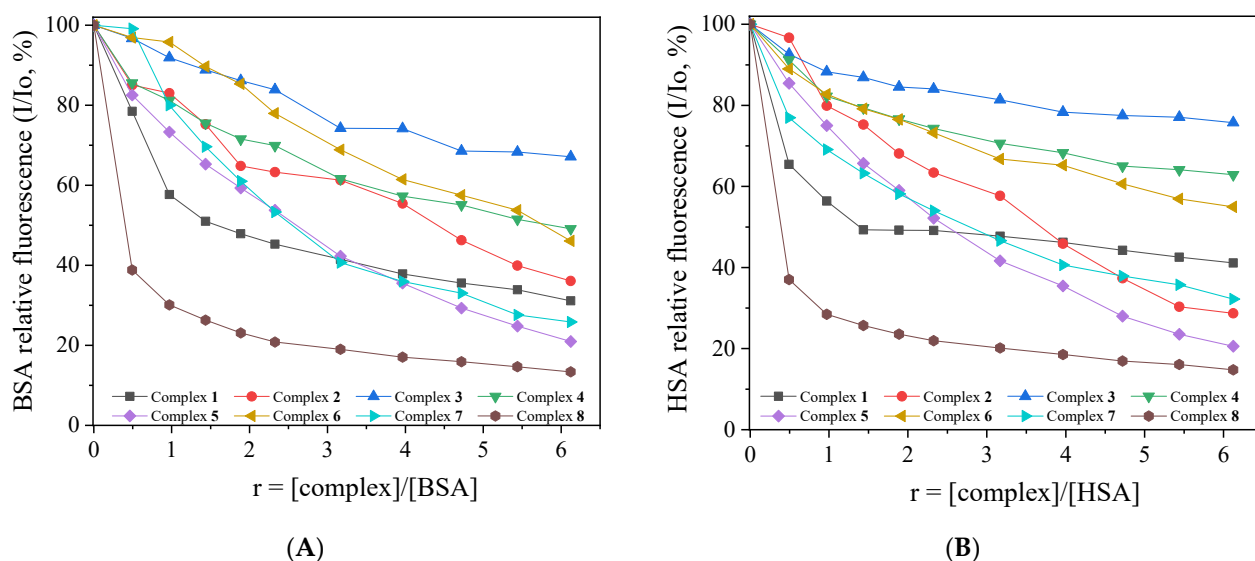


Figure 6. (A) Plot of % relative fluorescence intensity of BSA at $\lambda_{em} = 344$ nm (I/I_0 , %) versus r ($r = [\text{complex}]/[\text{BSA}]$) complexes 1–8 (up to 31.1% of the initial BSA fluorescence 1; 36.1% for 2; 67.1% for 3; 49.1% for 4; 20.9% for 5; 46.1% for 6; 25.8% for 7; and 13.4% for 8). (B) Plot of % relative fluorescence intensity of HSA at $\lambda_{em} = 342$ nm (I/I_0 , %) versus r ($r = [\text{complex}]/[\text{HSA}]$) for complexes 1–8 (up to 41.1% of the initial HSA fluorescence for 1; 28.7% for 2; 75.7% for 3; 62.9% for 4; 20.6% for 5; 54.9% for 6; 32.2% for 7; and 14.7% for 8).

Stern-Volmer and Scatchard equations (Equations (S2), (S3) and (S9)) and plots (Figures S14–S17) were used to calculate the corresponding SA-quenching constants (K_q) and the SA-binding (K) constants, respectively. For the calculation of K_q , the fluorescence lifetime of tryptophan in SA is $\tau_0 = 10^{-8}$ s [78]. For all compounds, the calculated K_q values (Table 4) are approximately two–three orders higher than the value $10^{10} \text{ M}^{-1} \text{ s}^{-1}$. Therefore, a static quenching mechanism may be suggested [78] to confirm the interaction of the compounds with the albumins. Regarding the K values, they are of the 10^4 – 10^6 M^{-1} order and are in the range found for other metal complexes with substituted salicylaldehydes [27,29,30,32–34,36–39]. All complexes 1–8 have K values lower than 10^{15} M^{-1} , which is the association constant of avidin with diverse compounds and is considered the highest of known noncovalent interactions. Such values show the reversible binding of SAs with the complexes, which, therefore, can be transferred and released to the desired bio-targets [89].

The identification of the albumin binding site of a compound is often required to understand their interaction. According to crystallography, the key sites for the attachment of drugs and metal ions are Sudlow's site one (or drug site I) in subdomain IIA and Sudlow's site two (or drug site II) in subdomain IIIA. In order to study the binding selectivity of the compounds towards these albumin-binding sites, warfarin and ibuprofen are used as site markers, respectively [90]. For this purpose, titration fluorescence quenching studies were performed in the presence of warfarin or ibuprofen (Figures S18–S21), and the corresponding K values for the compounds were calculated (Table 4) with the Scatchard equation (Equation (S9)) and corresponding plots (Figures S22–S25). If the presence of a marker influences the binding of the compound competitively (i.e., both the marker and the

compound bind in the same binding site), then a decrease in the corresponding K value will be observed, indicating the selectivity for the same binding site of respective marker [90].

Table 4. The SA-quenching constants (K_q , in $M^{-1} s^{-1}$) and the SA-binding constants in the absence or presence of the albumin site markers ibuprofen and warfarin (K, in M^{-1}) calculated for complexes 1–8.

| Compound | $K_q(\text{BSA}) (M^{-1} s^{-1})$ | $K(\text{BSA}) (M^{-1})$ | $K(\text{BSA,ibuprofen}) (M^{-1})$ | $K(\text{BSA,warfarin}) (M^{-1})$ |
|--|-----------------------------------|------------------------------|------------------------------------|-----------------------------------|
| [Fe(1naph-salo) ₃], 1 | $8.94(\pm 0.28) \times 10^{12}$ | $4.42(\pm 0.26) \times 10^5$ | $8.57(\pm 0.24) \times 10^4$ | $8.73(\pm 0.42) \times 10^4$ |
| {K[Fe(ovan) ₃] ₂ }Cl, 2 | $9.28(\pm 0.38) \times 10^{12}$ | $6.07(\pm 0.34) \times 10^4$ | $1.15(\pm 0.03) \times 10^5$ | $2.57(\pm 0.16) \times 10^4$ |
| [Fe(5Me-salo) ₃], 3 | $2.78(\pm 0.05) \times 10^{12}$ | $3.39(\pm 0.25) \times 10^4$ | $5.99(\pm 0.20) \times 10^4$ | $5.38(\pm 0.22) \times 10^4$ |
| [Fe(3EtO-salo) ₃], 4 | $5.41(\pm 0.17) \times 10^{12}$ | $1.15(\pm 0.04) \times 10^5$ | $7.10(\pm 0.16) \times 10^4$ | $3.75(\pm 0.19) \times 10^4$ |
| [Fe(4OH-salo) ₃], 5 | $1.81(\pm 0.10) \times 10^{13}$ | $8.63(\pm 0.50) \times 10^4$ | $5.20(\pm 0.23) \times 10^4$ | $1.47(\pm 0.11) \times 10^5$ |
| [Fe(4MeO-salo) ₃], 6 | $6.03(\pm 0.24) \times 10^{12}$ | $7.02(\pm 0.54) \times 10^3$ | $2.15(\pm 0.11) \times 10^4$ | $2.85(\pm 0.23) \times 10^4$ |
| [Fe(4Et ₂ N-salo) ₃], 7 | $1.66(\pm 0.05) \times 10^{13}$ | $8.61(\pm 0.44) \times 10^4$ | $9.82(\pm 0.32) \times 10^4$ | $2.48(\pm 0.10) \times 10^4$ |
| [Fe(3,5diBr-salo) ₃], 8 | $2.54(\pm 0.09) \times 10^{13}$ | $1.21(\pm 0.04) \times 10^6$ | $1.31(\pm 0.10) \times 10^6$ | $1.33(\pm 0.08) \times 10^6$ |
| Compound | $K_q(\text{HSA}) (M^{-1} s^{-1})$ | $K(\text{HSA}) (M^{-1})$ | $K(\text{HSA,ibuprofen}) (M^{-1})$ | $K(\text{HSA,warfarin}) (M^{-1})$ |
| [Fe(1naph-salo) ₃], 1 | $4.22(\pm 0.14) \times 10^{12}$ | $9.99(\pm 0.23) \times 10^5$ | $7.13(\pm 0.23) \times 10^4$ | $1.44(\pm 0.05) \times 10^5$ |
| {K[Fe(ovan) ₃] ₂ }Cl, 2 | $8.23(\pm 0.49) \times 10^{12}$ | $3.67(\pm 0.25) \times 10^4$ | $5.11(\pm 0.13) \times 10^4$ | $2.17(\pm 0.06) \times 10^5$ |
| [Fe(5Me-salo) ₃], 3 | $1.22(\pm 0.06) \times 10^{12}$ | $2.17(\pm 0.12) \times 10^5$ | $4.56(\pm 0.24) \times 10^4$ | $1.98(\pm 0.07) \times 10^5$ |
| [Fe(3EtO-salo) ₃], 4 | $2.47(\pm 0.12) \times 10^{12}$ | $1.45(\pm 0.07) \times 10^5$ | $5.11(\pm 0.20) \times 10^4$ | $2.13(\pm 0.07) \times 10^5$ |
| [Fe(4OH-salo) ₃], 5 | $2.08(\pm 0.13) \times 10^{13}$ | $8.03(\pm 0.23) \times 10^4$ | $5.46(\pm 0.29) \times 10^4$ | $1.83(\pm 0.06) \times 10^5$ |
| [Fe(4MeO-salo) ₃], 6 | $4.23(\pm 0.15) \times 10^{12}$ | $8.48(\pm 0.55) \times 10^4$ | $1.82(\pm 0.02) \times 10^4$ | $2.01(\pm 0.05) \times 10^5$ |
| [Fe(4Et ₂ N-salo) ₃], 7 | $1.09(\pm 0.03) \times 10^{13}$ | $1.52(\pm 0.07) \times 10^5$ | $5.20(\pm 0.05) \times 10^4$ | $3.29(\pm 0.10) \times 10^5$ |
| [Fe(3,5diBr-salo) ₃], 8 | $2.01(\pm 0.05) \times 10^{13}$ | $1.99(\pm 0.09) \times 10^6$ | $1.24(\pm 0.05) \times 10^6$ | $1.71(\pm 0.14) \times 10^6$ |

In the case of BSA, complexes 2, 4, and 7 present significantly lower K values in the presence of warfarin, which suggests that they have a binding selectivity for drug site I. On the other hand, complex 5 exhibits a lower K value in the presence of the ibuprofen marker, indicating a preference to bind to Sudlow's site II. For complexes 1, 3, 6, and 8, a safe conclusion concerning the binding preference for sites I or II is not obvious since the $K_{(\text{marker})}$ values are similar. Regarding HSA, all complexes 1–8 present significantly lower K values in the presence of ibuprofen, suggesting their selective attachment to Sudlow's site II.

2.6. Antioxidant Activity of the Complexes

Free radicals are reactive chemical species with unpaired electron(s) and may usually induce inflammations [91]. They are produced as part of mitochondrial metabolism and may attack DNA, proteins, and lipids. On the counterpart, antioxidants are compounds that delay or prevent the oxidation of these substrates [92]. Natural antioxidants are usually organic compounds such as phenolic acids, flavones, and flavonoids. However, a combination of the redox properties of metal ions with various ligands may lead to effective metal-based antioxidant compounds [92]. Within this context, the ability of complexes 1–8 to scavenge DPPH and ABTS radicals and to reduce H_2O_2 was studied and compared with the well-known antioxidant agents NDGA, BHT, trolox, and L-ascorbic acid, which are widely used standard reference antioxidants [93,94].

The ability of compounds to scavenge DPPH radicals is often related to preventing aging, cancer, and inflammation [95]. The method is based on the discoloration of the violet-colored methanolic solution of DPPH in the presence of the compounds [95]. The DPPH scavenging ability may also evaluate the antioxidant capacity of coordination compounds [92]. Most of the complexes under study are inactive or exhibit low activity towards DPPH radicals, which are found to be time-dependent for complexes 2 and 4 only (Table 5). Complex 2 is the most active compound herein towards DPPH radicals (%DPPH scaveng-

ing ability up to $49.03 \pm 0.71\%$) and is among the most active reported metal complexes of substituted salicylaldehydes [27,29,30,32,33,38,39]. All complexes 1–8 are less active than the reference compounds NDGA and BHT.

Table 5. %DPPH scavenging ability (DPPH%), %ABTS scavenging activity (ABTS %), and H₂O₂-reducing ability (H₂O₂%) for the compounds.

| Compound | DPPH% (30 min/60 min) | ABTS% | %H ₂ O ₂ |
|---|---------------------------|--------------|--------------------------------|
| [Fe(1naph-salo) ₃], 1 | 8.60 ± 0.62/6.46 ± 0.89 | 17.78 ± 0.53 | 68.69 ± 0.05 |
| {K[Fe(ovan) ₃] ₂ }Cl, 2 | 33.85 ± 0.17/49.03 ± 0.71 | 85.69 ± 0.67 | 54.30 ± 0.48 |
| [Fe(5Me-salo) ₃], 3 | 11.91 ± 0.11/11.18 ± 0.67 | 31.29 ± 0.62 | 44.04 ± 0.36 |
| [Fe(3EtO-salo) ₃], 4 | 23.70 ± 0.42/29.40 ± 0.71 | 78.62 ± 0.71 | 71.10 ± 0.06 |
| [Fe(4OH-salo) ₃], 5 | 0.86 ± 0.34/2.62 ± 0.45 | 84.72 ± 0.76 | 72.28 ± 0.19 |
| [Fe(4MeO-salo) ₃], 6 | 4.83 ± 0.93/5.43 ± 0.27 | 11.05 ± 0.59 | 47.76 ± 0.61 |
| [Fe(4Et ₂ N-salo) ₃], 7 | Not active | 57.07 ± 0.67 | 49.46 ± 0.51 |
| [Fe(3,5diBr-salo) ₃], 8 | Not active | 60.39 ± 0.53 | 85.86 ± 0.89 |
| BHT | 70.23 ± 0.95/88.60 ± 0.27 | Not tested | Not tested |
| NDGA | 93.51 ± 0.12/93.54 ± 0.11 | Not tested | Not tested |
| Trolox | Not tested | 89.25 ± 0.11 | Not tested |
| L-ascorbic acid | Not tested | Not tested | 60.51 ± 0.54 |

The ability of a compound to scavenge the cationic ABTS radicals (ABTS^{•+}) is used as a marker of the total antioxidant activity [95]. The assay is based on the discoloration of a dark green solution with the cationic radical ABTS^{•+}, which is induced by the compounds [95]. The ABTS scavenging ability is low-to-moderate. Such differentiation of the ABTS scavenging ability depends on the nature of X-saloH as it was previously reported for Mn(II), Cu(II), Zn(II), Pd(II), and Gd(III) complexes with substituted salicylaldehydes [27,29,30,32,33,38,39]. However, the activity of the most active compounds, namely complexes **2** and **5** ($= 85.69 \pm 0.67\%$ and $84.72 \pm 0.76\%$, respectively), was close to the activity of the reference compound trolox (Table 5).

The interaction of the compounds with hydrogen peroxide (which produces hydroxyl radicals) may serve as a marker of inhibition of reactive oxygen species, offering protection from oxidative stress [96]. The ability of complexes 1–8 to reduce H₂O₂ is comparable with that of reference compound L-ascorbic acid (Table 5). Complex **8** presents the highest percentage of H₂O₂ reduction (H₂O₂% = $85.86 \pm 0.89\%$) and is the most active among the compounds under study. The behavior of the complexes is similar to that reported for a series of Mn(II), Cu(II), Zn(II), Pd(II), and Gd(III) complexes with substituted salicylaldehydes [27,29,30,32,33,38,39].

In total, complexes 1–8 were practically inactive towards DPPH radicals except for complex **2**, which presented a moderate DPPH scavenging activity. Regarding ABTS radicals, only complexes **2** and **5** approached the activity of the reference compound trolox. All complexes studied herein exhibited toward hydrogen peroxide comparable activity with the reference compound L-ascorbic acid, with complex **8** being the most active compound.

3. Materials and Methods

3.1. Materials-Instrumentation-Physical Measurements

All chemicals and solvents were reagent grade and were used as purchased from commercial sources: sodium citrate, NaCl, CT DNA, EB, BSA, HSA, and ABTS were purchased from Sigma-Aldrich Co; BHT, NDGA, K₂S₂O₈, and trolox were purchased from J&K Scientific Co; 1naph-saloH, ovanH, 5Me-saloH, 3EtO-saloH, 4OH-saloH, 4MeO-saloH, 4Et₂N-saloH, sodium warfarin, ibuprofen, and DPPH were purchased from Tokyo Chemical industry (TCI); 3,5diBr-saloH was purchased from Fluorochem; Tris base, EDTA disodium

salt dehydrate, loading buffer, and H₂O₂ (30% *w/v*) were purchased from PanReac AppliChem ITW Reagents Co; supercoiled circular pBR322 plasmid DNA was purchased from New England Bioline; FeCl₃·6H₂O, CH₃ONa, KOH, L-ascorbic acid, Na₂HPO₄, NaH₂PO₄, HCl (35% *v/v*) and all solvents were purchased from Chemlab Co.

The DNA stock solution was prepared by the dilution of CT DNA to a buffer solution (containing 150 mM NaCl and 15 mM sodium citrate at pH 7.0) followed by stirring at 4 °C and was kept at 4 °C for no longer than two weeks. The stock solution of CT DNA gave a ratio of UV absorbance at 260 and 280 nm (A_{260}/A_{280}) in the range of 1.88–1.90, indicating that DNA was sufficiently free of protein contamination [97]. The DNA concentration was determined by the UV absorbance at 260 nm after a 1:20 dilution using $\epsilon = 6600 \text{ M}^{-1} \text{ cm}^{-1}$ [98].

Infrared (IR) spectra were obtained on a Thermo Scientific Nicolet iS20 FTIR ATR spectrometer without any treatment of the solid sample in the range of 400–4000 cm⁻¹ (abbreviations used included vs. = very strong; s = strong; sm = strong-to-medium; and m = medium). The UV-vis spectra were recorded in the range 200–800 nm as solid and in solution (concentrations in the range of 10 μM–1 mM) on a Jasco V-750 spectrophotometer (abbreviation used included sh = shoulder). The spectra were recorded in DMSO solutions using quartz cells with an optical path of 1 cm sealed tightly with Teflon caps. The fluorescence emission spectra were recorded in solution in quartz cells (1 cm) on a Hitachi F-7000 fluorescence spectrophotometer. C, H, and N elemental analyses were performed on a Perkin Elmer 240B elemental analyzer. The molar conductivity measurements were carried out on a 1 mM DMSO solution of the complexes with a Crison Basic 30 conductometer. The viscosity experiments were conducted using an ALPHA L Fungilab rotational viscometer equipped with an 18 mL LCP spindle.

3.2. Synthesis of the Complexes

All complexes were prepared at room temperature according to the following procedure: KOH (0.3 mmol, 300 μL of 1 M solution) or CH₃ONa (0.3 mmol, 16 mg) was added into a methanolic solution (5–10 mL) of the corresponding X-saloH (0.3 mmol) under stirring for 45 min in order to deprotonate the X-saloH. Afterward, the resultant solution was added dropwise to a methanolic solution of FeCl₃·6H₂O (0.1 mmol, 27 mg). The final solution was stirred for an additional 45 min, then was filtered and left to evaporate slowly at room temperature. After a few days, the desired product was suspended in a minimal amount of methanol and filtered and washed with water and diethyl ether or dichloromethane.

[Fe(1naph-salo)₃] (1): For the synthesis of complex **1**, 1naph-saloH (0.3 mmol, 52 mg) was the corresponding X-saloH and was deprotonated with CH₃ONa (0.3 mmol, 16 mg). After ten days, red-brown single crystals of [Fe(1naph-salo)₃] suitable for X-ray structural determination were collected (Yield: 40 mg, 70%). Anal. calcd. for C₃₃H₂₁FeO₆ (MW = 569.37): C 69.61, H 3.72; found C 69.42, H 3.61%. FT-IR (ATR), $\nu_{\text{max}}/\text{cm}^{-1}$: $\nu(\text{C}=\text{O})_{\text{aldehydo}}$, 1614 (s); $\nu(\text{C}-\text{O})_{\text{phenolato}}$, 1306 (m). UV-vis: solid, λ/nm : 510, 410; in DMSO, λ/nm ($\epsilon/\text{M}^{-1} \text{ cm}^{-1}$): 501 (190), 425 (5900), 410 (6300), 368 (4500), 306 (sh) (7000), 298 (sh) (7900), 269 (12,500). Complex **1** is soluble in DMF and DMSO ($\Lambda_{\text{M}} = 11 \text{ mho}\cdot\text{cm}^2\cdot\text{mol}^{-1}$, 1 mM DMSO) and partially soluble in methanol.

{K[Fe(ovan)₃]₂}Cl·MeOH (2): For the synthesis of complex **2**, KOH (0.3 mmol, 300 μL of 1 M solution) deprotonated ovanH (0.3 mmol, 46 mg) which was the corresponding X-saloH. Dark-red single crystals of {K[Fe(ovan)₃]₂}Cl·MeOH suitable for X-ray structural determination were collected after a week (Yield: 90 mg, 80%). Anal. calcd. for C₄₉H₄₆ClFe₂KO₁₉ (MW = 1125.14): C 52.31, H 4.12; found C 52.15, H 4.30%. FT-IR (ATR), $\nu_{\text{max}}/\text{cm}^{-1}$: $\nu(\text{C}=\text{O})_{\text{aldehydo}}$, 1626 (m); $\nu(\text{C}-\text{O})_{\text{phenolato}}$, 1313 (m). UV-vis: solid,

λ/nm : 510, 405; in DMSO, λ/nm ($\epsilon/M^{-1}\text{ cm}^{-1}$): 475(sh) (300), 385(sh) (3500), 355 (7500), 320 (6500), 278 (6700). Complex 2 is soluble in DMF and DMSO ($\Lambda_M = 15\text{ mho}\cdot\text{cm}^2\cdot\text{mol}^{-1}$, 1 mM DMSO).

[Fe(5Me-salo)₃] (3): For the synthesis of complex 3, CH₃ONa (0.3 mmol, 16 mg) was used for the deprotonation of the corresponding X-saloH, namely 5Me-saloH (0.3 mmol, 41 mg). After two weeks, the formation of the dark-red precipitate of [Fe(5Me-salo)₃] was observed and the product was collected with filtration and washed with water and diethyl ether (Yield: 30 mg, 30%). Anal. calcd. for C₂₄H₂₁FeO₆ (MW = 461.27): C 62.49, H 4.59; found: C 62.25, H 4.33%. FT-IR (ATR), $\nu_{\text{max}}/\text{cm}^{-1}$: $\nu(\text{C}=\text{O})_{\text{aldehyde}}$, 1622 (s); $\nu(\text{C}-\text{O})_{\text{phenolato}}$, 1312 (sm). UV-vis: solid, λ/nm : 498, 415; in DMSO, λ/nm ($\epsilon/M^{-1}\text{ cm}^{-1}$): 518 (sh) (200), 410 (400), 335 (5600). Complex 3 is soluble in DMF and DMSO ($\Lambda_M = 11\text{ mho}\cdot\text{cm}^2\cdot\text{mol}^{-1}$, 1 mM DMSO) and partially soluble in methanol.

[Fe(3EtO-salo)₃] (4): For the synthesis of complex 4, the deprotonation of 3EtO-saloH (0.3 mmol, 50 mg), the corresponding X-saloH, was achieved with CH₃ONa (0.3 mmol, 16 mg). The dark-red precipitate of [Fe(3EtO-salo)₃] was collected with filtration and washed with water and diethyl ether (Yield: 40 mg, 72%) after two weeks. Anal. calcd. for C₂₇H₂₇FeO₉ (MW = 551.35): C 58.82, H 4.94; found C 58.55, H 5.09%. FT-IR (ATR), $\nu_{\text{max}}/\text{cm}^{-1}$: $\nu(\text{C}=\text{O})_{\text{aldehyde}}$, 1600 (vs); $\nu(\text{C}-\text{O})_{\text{phenolato}}$, 1319 (sm). UV-vis: solid, λ/nm : 517; in DMSO, λ/nm ($\epsilon/M^{-1}\text{ cm}^{-1}$): 519 (250), 405 (2700), 340 (7500), 272 (sh) (16,000). Complex 4 is soluble in DMF and DMSO ($\Lambda_M = 15\text{ mho}\cdot\text{cm}^2\cdot\text{mol}^{-1}$, 1 mM DMSO) and partially soluble in methanol.

[Fe(4OH-salo)₃] (5): For the synthesis of complex 5, 4OH-saloH (0.3 mmol, 41 mg) was the corresponding X-saloH and was deprotonated with CH₃ONa (0.3 mmol, 16 mg). The red-brown precipitate of [Fe(4OH-salo)₃] was collected with filtration and washed with water and diethyl ether after a few days (Yield: 40 mg, 85%). Anal. calcd. for C₂₁H₁₅FeO₉ (MW = 467.19): C 53.99, H 3.24; found C 54.15, H 3.45%. FT-IR (ATR), $\nu_{\text{max}}/\text{cm}^{-1}$: $\nu(\text{C}=\text{O})_{\text{aldehyde}}$, 1615 (m); $\nu(\text{C}-\text{O})_{\text{phenolato}}$, 1324 (s). UV-vis: solid, λ/nm : 495; in DMSO, λ/nm ($\epsilon/M^{-1}\text{ cm}^{-1}$): 505(sh) (190), 353(sh) (4500), 316 (15,000), 280 (1800). Complex 5 is soluble in DMF and DMSO ($\Lambda_M = 10\text{ mho}\cdot\text{cm}^2\cdot\text{mol}^{-1}$, 1 mM DMSO) and partially soluble in methanol.

[Fe(4MeO-salo)₃] (6): For the synthesis of complex 6, CH₃ONa (0.3 mmol, 16 mg) was used to deprotonate the corresponding X-saloH, i.e., 4MeO-saloH (0.3 mmol, 46 mg). After a few days, a dark-red product of [Fe(4MeO-salo)₃] was collected with filtration and washed with water and diethyl ether (Yield: 25 mg, 49%). Anal. calcd. for C₂₄H₂₁FeO₉ (MW = 509.27): C 56.60, H 4.16; found C 56.45, H 4.32%. FT-IR (ATR), $\nu_{\text{max}}/\text{cm}^{-1}$: $\nu(\text{C}=\text{O})_{\text{aldehyde}}$, 1625 (m); $\nu(\text{C}-\text{O})_{\text{phenolato}}$, 1307 (m). UV-vis: solid, λ/nm : 465; in DMSO, λ/nm ($\epsilon/M^{-1}\text{ cm}^{-1}$): 485 (350), 403 (1800), 318(sh) (9800), 285 (15,700). Complex 6 is soluble in DMF and DMSO ($\Lambda_M = 14\text{ mho}\cdot\text{cm}^2\cdot\text{mol}^{-1}$, 1 mM DMSO) and partially soluble in methanol.

[Fe(4Et₂N-salo)₃] (7): For the synthesis of complex 7, the corresponding X-saloH was 4Et₂N-saloH (0.3 mmol, 58 mg) and was dissolved in a 1:1 CH₃OH/CH₂Cl₂ mixture (10 mL). 4Et₂N-saloH was deprotonated with KOH (0.3 mmol, 300 μL of 1 M solution). After two weeks, the dark-red precipitate of [Fe(4Et₂N-salo)₃] was collected with filtration and washed with water and dichloromethane (Yield: 50 mg, 79%). Anal. calcd. for C₃₃H₄₂FeN₃O₆ (MW = 632.56): C 62.66, H 6.69, N 6.64; found C 62.41, H 6.43, N 6.47%. FT-IR (ATR), $\nu_{\text{max}}/\text{cm}^{-1}$: $\nu(\text{C}=\text{O})_{\text{aldehyde}}$, 1615 (s); $\nu(\text{C}-\text{O})_{\text{phenolato}}$, 1315 (sm). UV-vis: solid, λ/nm : 495, 403; in DMSO, λ/nm ($\epsilon/M^{-1}\text{ cm}^{-1}$): 485 (600), 407 (5100), 350 (15,300), 267 (sh) (8900). Complex 7 is soluble in DMF and DMSO ($\Lambda_M = 12\text{ mho}\cdot\text{cm}^2\cdot\text{mol}^{-1}$, 1 mM DMSO) and partially soluble in methanol.

[Fe(3,5diBr-salo)₃] (8): For the synthesis of complex **8**, CH₃ONa (0.3 mmol, 16 mg) was used for the deprotonation of 3,5diBr-saloH (0.3 mmol, 84 mg) which was used as the corresponding X-saloH. A small quantity (5 mL) of hexane was added for slow vapor diffusion. The orange microcrystalline product of [Fe(3,5diBr-salo)₃] (**8**) was formed after two weeks, collected with filtration, and washed with water and diethyl ether (Yield: 50 mg, 56%). Anal. calcd. for C₂₁H₉Br₆FeO₆ (MW = 892.60): C 28.26, H 1.02; found C 28.52, H 1.18%. FT-IR (ATR), $\nu_{\max}/\text{cm}^{-1}$: $\nu(\text{C}=\text{O})_{\text{aldehyde}}$, 1606 (vs); $\nu(\text{C}-\text{O})_{\text{phenolato}}$, 1311 (sm). UV-vis: solid, λ/nm : 498, 405; in DMSO, λ/nm ($\epsilon/\text{M}^{-1}\text{cm}^{-1}$): 500(sh) (250), 427 (500), 320 (1400), 294 (10,700), 268 (4000). Complex **8** is soluble in DMF and DMSO ($\Lambda_{\text{M}} = 16\text{ mho}\cdot\text{cm}^2\cdot\text{mol}^{-1}$, 1 mM DMSO) and partially soluble in methanol.

3.3. Single-Crystal X-Ray Crystallography

Suitable single crystals of compounds **1** and **2** were mounted on thin glass fibers with the aid of epoxy resin. X-ray diffraction data were recorded on a Bruker Kappa Apex II CCD area-detector diffractometer equipped with a Mo K α ($\lambda = 0.71073\text{ \AA}$, sealed tube source operating at 50 kV and 30 mA) and a Triumph monochromator at 295 K, using the φ and ω scanning technique. The program Apex2 (Bruker AXS, 2006) was used for data collection and cell refinement. The collected data were integrated with the Bruker SAINT software package [99] using a narrow frame algorithm. Data were corrected for absorption using the numerical method SADABS [100] based on the crystal dimensions. Structures were solved using the SUPERFLIP package [101] and refined with full-matrix least squares on F^2 using the Crystals program package version 14.61 build 6236 [102]. Anisotropic displacement parameters were applied for all non-hydrogen, non-disordered atoms.

For the disordered atoms in the case of complex **2**, their occupation factors under fixed isotropic thermal parameters were first detected. Afterward, all were refined with fixed occupation factors isotropically in the case of methanol solvent molecules and anisotropically in the case of the chloride counter anion. Hydrogen atoms were, in general, found and/or positioned geometrically and refined using a riding model with the isotropic displacement parameters $\text{Uiso}(\text{H}) = 1.2\text{Ueq}(\text{C})$ or $1.5\text{Ueq}(\text{methyl and }-\text{OH hydrogens})$ at distances of C–H 0.95 \AA and O–H 0.82 \AA . All methyl and OH hydrogen atoms were allowed to rotate. Hydrogen atoms riding on disordered oxygen atoms of methanol solvent molecules were positioned geometrically to fulfill hydrogen bonding demands. Details of crystal data and structure refinement parameters are shown in Table S1.

CCDC deposition numbers 2447090 and 2447091 contain the supplementary crystallographic data for complexes **1** and **2**. These data can be obtained free of charge via <https://www.ccdc.cam.ac.uk/>, accessed on 26 May 2025 (or from the Cambridge Crystallographic Data Centre, 12 Union Road, Cambridge CB21EZ, UK; fax: (+44) 1223-336-033; or deposit@ccdc.cam.ac.uk).

3.4. Study of the Biological Profile of the Complexes

The in vitro evaluation of the biological activity of the complexes, i.e., their interaction with CT DNA and albumins, was conducted following the dissolution of the complexes in DMSO (1 mM) because of their limited solubility in water. The experiments were conducted in the presence of aqueous buffer solutions, ensuring that the ratio of DMSO in the final solution did not exceed 5% (v/v). Control experiments were implemented to evaluate the impact of DMSO on the data. Minimal or no alterations were observed in the spectra of albumins or CT DNA, and appropriate adjustments were made when necessary.

All the procedures and relevant equations used in the in vitro study of the biological activity (interactions with CT DNA, pDNA, HSA, and BSA, and antioxidant activity) of the compounds are described in the Supporting Information file (Sections S1–S4).

4. Conclusions

Eight novel homoleptic iron(III) complexes with a series of substituted salicylaldehydes as ligands were synthesized and characterized by diverse techniques. For all complexes, the general formula $[\text{Fe}(\text{X-salo})_3]$ was suggested where the X-salo ligands are bound to Fe(III) ion in a bidentate chelating fashion the aldehyde and the phenolato-oxygen atoms. The crystal structures of complexes **1** and **2** were determined by single-crystal X-ray crystallography. In the structure of complex **2**, a potassium cation was hosted in the space generated between two $[\text{Fe}(\text{ovan})_3]$ moieties interacting with the methoxy and oxygen atoms of the *o*-vanillin ligands.

The complexes interacted with CT DNA in an intercalative manner, with complex **1** bearing the highest DNA-binding constant ($1.62(\pm 0.01) \times 10^7 \text{ M}^{-1}$), which could be attributed to the extended aromatic system of the 1naph-salo ligand. The ability of the complexes to cleave pBR322 plasmid DNA to relaxed circular DNA is moderate at a concentration of 500 μM in the absence of irradiation, but it is highly enhanced upon irradiation, especially with UVA and UVB light.

The complexes may bind tightly and reversibly to bovine and human serum albumin and may become transferred to potential biological targets. Competitive studies with the reference site markers ibuprofen and warfarin showed that in the case of HSA, complexes **1–8** seemed to bind selectively at Sudlow's site II. Regarding BSA, complexes **2, 4, and 7** prefer binding at Sudlow's site I and complex **5** at Sudlow's site II.

Regarding the antioxidant activity of the complexes, the ability to scavenge DPPH and ABTS radicals and to reduce H_2O_2 was examined. Almost all complexes were more inactive towards DPPH radicals except for complex **2**, which presented a moderate and time-dependent DPPH scavenging activity (%DPPH = 33.85 ± 0.17 – $49.03 \pm 0.71\%$). The complexes showed a low-to-moderate ability to scavenge ABTS radicals, with the most active complexes **2** and **5** approaching the activity of the reference compound trolox. Concerning the activity towards H_2O_2 , most complexes were found to be more active than the reference compound L-ascorbic acid, with complex **8** being the most active ($\text{H}_2\text{O}_2\%$ = $85.86 \pm 0.89\%$).

Such features may be useful and, with the aid of more elaborate biological assays, could reveal alternative pathways regarding the potential use of these types of compounds as pharmaceutical agents.

Supplementary Materials: The following supporting information can be downloaded at <https://www.mdpi.com/article/10.3390/molecules30112383/s1>. Cif and checkcif files for compounds **1** and **2**. Protocols and equations regarding binding studies with CT DNA (S1), pDNA cleavage studies (S2), albumin-binding studies (S3), and antioxidant activity assay (S4) [103–105]. Tables S1–S4 and Figures S1–S25 are included in the ESI file.

Author Contributions: Conceptualization, Z.P. and G.P.; methodology, Z.P., A.G.H. and G.P.; formal analysis, Z.P., A.G.H. and G.P.; investigation, Z.P., A.G.H. and G.P.; resources, A.G.H. and G.P.; data curation, Z.P., A.G.H. and G.P.; writing—original draft preparation, Z.P., A.G.H. and G.P.; writing—review and editing, Z.P., A.G.H. and G.P.; supervision, G.P.; project administration, G.P.; funding acquisition, G.P. All authors have read and agreed to the published version of the manuscript.

Funding: This research received no external funding.

Institutional Review Board Statement: Not applicable.

Informed Consent Statement: Not applicable.

Data Availability Statement: All necessary supplementary data are included in the supplementary files.

Conflicts of Interest: The authors declare no conflicts of interest.

Abbreviations

The following abbreviations are used in this manuscript:

| | |
|---------------|--|
| 1naph-saloH | 2-hydroxy-1-naphthaldehyde |
| 3,5diBr-saloH | 3,5-dibromo-salicylaldehyde |
| 3EtO-saloH | 3-ethoxy-salicylaldehyde |
| 4Et2N-saloH | 4-diethylamino-salicylaldehyde |
| 4MeO-saloH | 4-methoxy-salicylaldehyde |
| 4OH-saloH | 4-hydroxy-salicylaldehyde |
| 5Me-saloH | 5-methyl-salicylaldehyde |
| ABTS | 2,2'-azinobis-(3-ethylbenzothiazoline-6-sulfonic acid) |
| BHT | Butylated hydroxytoluene |
| BSA | Bovine serum albumin |
| CT | Calf thymus |
| DPPH | 1,1-diphenyl-picrylhydrazyl |
| EB | Ethidium bromide |
| HSA | Human serum albumin |
| K | SA-binding constant |
| Kb | DNA-binding constant |
| Kq | Quenching constant |
| KSV | Stern-Volmer constant |
| NDGA | Nordihydroguaiaretic acid |
| ovan | 3-methoxy-salicylaldehyde, o-vanillin |
| pDNA | pBR322 plasmid DNA |
| SA | Serum albumin |
| saloH | Salicylaldehyde |
| trolox | 6-hydroxy-2,5,7,8-tetramethylchroman-2-carboxylic acid |
| X-saloH | Substituted salicylaldehyde |

References

- Klimova, B.; Storek, M.; Valis, M.; Kuca, K. Global View on Rare Diseases: A Mini Review. *Curr. Med. Chem.* **2017**, *24*, 3153–3158. [[CrossRef](#)] [[PubMed](#)]
- Fermaglich, L.J.; Miller, K.L. A comprehensive study of the rare diseases and conditions targeted by orphan drug designations and approvals over the forty years of the Orphan Drug Act. *Orphanet J. Rare Dis.* **2023**, *18*, 163. [[CrossRef](#)]
- Abrams, M.J.; Murrer, B.A. Metal Compounds in Therapy and Diagnosis. *Science* **1993**, *261*, 725–730. [[CrossRef](#)]
- Karges, J.; Stokes, R.W.; Cohen, S.M. Metal complexes for therapeutic applications. *Trends Chem.* **2021**, *3*, 523–534. [[CrossRef](#)]
- Abbaspour, N.; Hurrell, R.; Kelishadi, R. Review on iron and its importance for human health. *J. Res. Med. Sci.* **2014**, *19*, 164.
- de Morais, T.R.; Gambero, A. Iron chelators in obesity therapy—Old drugs from a new perspective? *Eur. J. Pharmacol.* **2019**, *861*, 172614. [[CrossRef](#)] [[PubMed](#)]
- Sukhbaatar, N.; Weichhart, T. Iron Regulation: Macrophages in Control. *Pharmaceuticals* **2018**, *11*, 137. [[CrossRef](#)]
- Rout, G.R.; Sahoo, S. Role of iron in plant growth and metabolism. *Rev. Agric. Sci.* **2015**, *3*, 1–24. [[CrossRef](#)]
- Zhang, H.; Zhabyeyev, P.; Wang, S.; Oudit, G.Y. Role of iron metabolism in heart failure: From iron deficiency to iron overload. *Biochim. Biophys. Acta (BBA)-Mol. Basis Dis.* **2019**, *1865*, 1925–1937. [[CrossRef](#)]
- Lieu, P.T.; Heiskala, M.; Peterson, P.A.; Yang, Y. The roles of iron in health and disease. *Mol. Asp. Med.* **2001**, *22*, 1–87. [[CrossRef](#)]
- Ying, J.-F.; Lu, Z.-B.; Fu, L.-Q.; Tong, Y.; Wang, Z.; Li, W.-F.; Mou, X.-Z. The role of iron homeostasis and iron-mediated ROS in cancer. *Am. J. Cancer Res.* **2021**, *11*, 1895. [[PubMed](#)] [[PubMed Central](#)]
- Kuang, Y.; Wang, Q. Iron and lung cancer. *Cancer Lett.* **2019**, *464*, 56–61. [[CrossRef](#)] [[PubMed](#)]
- Vessieres, A. Iron Compounds as Anticancer Agents. In *Metal-Based Anticancer Agents*; Casini, A., Vessieres, A., Meier-Menches, S.M., Eds.; Royal Society of Chemistry: London, UK, 2019; pp. 62–90. [[CrossRef](#)]
- Arias, L.S.; Pessan, J.P.; Vieira, A.P.M.; De Lima, T.M.T.; Delbem, A.C.B.; Monteiro, D.R. Iron Oxide Nanoparticles for Biomedical Applications: A Perspective on Synthesis, Drugs, Antimicrobial Activity, and Toxicity. *Antibiotics* **2018**, *7*, 46. [[CrossRef](#)]
- Lin, J.F.; Wu, C.C.; Liao, Y.J.; Jakfar, S.; Tang, Z.B.; Chen, J.K.; Lin, F.H. In Vitro and In Vivo Evaluations of Mesoporous Iron Particles for Iron Bioavailability. *Int. J. Mol. Sci.* **2019**, *20*, 5291. [[CrossRef](#)]

16. Wani, W.A.; Baig, U.; Shreaz, S.; Shiekh, R.A.; Iqbal, P.F.; Jameel, E.; Ahmad, A.; Mohd-Setapar, S.H.; Mushtaque, M.; Hun, L.T. Recent advances in iron complexes as potential anticancer agents. *New J. Chem.* **2016**, *40*, 1063–1090. [[CrossRef](#)]
17. Naureen, B.; Miana, G.A.; Shahid, K.; Asghar, M.; Tanveer, S.; Sarwar, A. Iron (III) and zinc (II) monodentate Schiff base metal complexes: Synthesis, characterisation and biological activities. *J. Mol. Struct.* **2021**, *1231*, 129946. [[CrossRef](#)]
18. Dimitrakopoulou, A.; Dendrinou-Samara, C.; Pantazaki, A.A.; Raptopoulou, C.; Terzis, A.; Samaras, E.; Kessissoglou, D.P. Interaction of Fe(III) with herbicide-carboxylate ligands. Di-, tri- and tetra-nuclear compounds: Structure, antimicrobial study and DNA interaction. *Inorganica Chim. Acta* **2007**, *360*, 546–556. [[CrossRef](#)]
19. Dong, Y.R.; Cheng, S.J.; Qi, G.H.; Yang, Z.P.; Yin, S.Y.; Chen, G.T. Antimicrobial and antioxidant activities of *Flammulina velutipes* polysaccharides and polysaccharide-iron(III) complex. *Carbohydr. Polym.* **2017**, *161*, 26–32. [[CrossRef](#)]
20. Adjimani, J.P.; Asare, P. Antioxidant and free radical scavenging activity of iron chelators. *Toxicol. Rep.* **2015**, *2*, 721–728. [[CrossRef](#)]
21. Dimiza, F.; Barmpa, A.; Chronakis, A.; Hatzidimitriou, A.G.; Sanakis, Y.; Papadopoulos, A.N.; Psomas, G. Iron(III) Complexes with Non-Steroidal Anti-Inflammatory Drugs: Structure, Antioxidant and Anticholinergic Activity, and Interaction with Biomolecules. *Int. J. Mol. Sci.* **2023**, *24*, 6391. [[CrossRef](#)]
22. Dimiza, F.; Hatzidimitriou, A.G.; Sanakis, Y.; Papadopoulos, A.N.; Psomas, G. Trinuclear and tetranuclear iron(III) complexes with fenamates: Structure and biological profile. *J. Inorg. Biochem.* **2021**, *218*, 111410. [[CrossRef](#)]
23. Michalski, C.; Mohagheghi, H.; Nimtz, M.; Pasteels, J.; Ober, D. Salicyl Alcohol Oxidase of the Chemical Defense Secretion of Two Chrysomelid Leaf Beetles. *J. Biol. Chem.* **2008**, *283*, 19219–19228. [[CrossRef](#)]
24. Pelttari, E.; Lehtinen, M.; Elo, H. Substituted salicylaldehydes as potential antimicrobial drugs: Minimal inhibitory and microbicidal concentrations. *Z. Fur Naturforschung-Sect. C J. Biosci.* **2011**, *66*, 571–580. [[CrossRef](#)] [[PubMed](#)]
25. Pelttari, E.; Karhumaki, E.; Langshaw, J.; Perakyla, H.; Elo, H. Antimicrobial properties of substituted salicylaldehydes and related compounds. *Z. Fur Naturforschung-Sect. C J. Biosci.* **2007**, *62*, 487–497. [[CrossRef](#)]
26. Bountagkidou, O.G.; Ordoudi, S.A.; Tsimidou, M.Z. Structure-antioxidant activity relationship study of natural hydroxybenzaldehydes using in vitro assays. *Food Res. Int.* **2010**, *43*, 2014–2019. [[CrossRef](#)]
27. Ntanatsidis, S.; Perontsis, S.; Konstantopoulou, S.; Kalogiannis, S.; Hatzidimitriou, A.G.; Papadopoulos, A.N.; Psomas, G. Manganese(II) complexes of substituted salicylaldehydes and α -diimines: Synthesis, characterization and biological activity. *J. Inorg. Biochem.* **2022**, *227*, 111693. [[CrossRef](#)] [[PubMed](#)]
28. Psarras, G.I.; Zianna, A.; Hatzidimitriou, A.G.; Psomas, G. Coordination Compounds of Nickel(II) with 3,5-Dibromo-Salicylaldehyde: Structure and Interaction with Biomolecules. *Inorganics* **2024**, *12*, 138. [[CrossRef](#)]
29. Papadopoulos, Z.; Doulopoulou, E.; Zianna, A.; Hatzidimitriou, A.G.; Psomas, G. Copper(II) Complexes of 5-Fluoro-Salicylaldehyde: Synthesis, Characterization, Antioxidant Properties, Interaction with DNA and Serum Albumins. *Molecules* **2022**, *27*, 8929. [[CrossRef](#)]
30. Zianna, A.; Geromichalos, G.; Fiotaki, A.M.; Hatzidimitriou, A.G.; Kalogiannis, S.; Psomas, G. Palladium(II) Complexes of Substituted Salicylaldehydes: Synthesis, Characterization and Investigation of Their Biological Profile. *Pharmaceuticals* **2022**, *15*, 886. [[CrossRef](#)]
31. Ristovic, M.S.; Zianna, A.; Psomas, G.; Hatzidimitriou, A.G.; Coutouli-Argyropoulou, E.; Lalia-Kantouri, M. Interaction of dinuclear cadmium(II) 5-Cl-salicylaldehyde complexes with calf-thymus DNA. *Mater. Sci. Eng. C* **2016**, *61*, 579–590. [[CrossRef](#)]
32. Gkisiou, C.; Malis, G.; Hatzidimitriou, A.G.; Psomas, G. Erbium(III) coordination compounds with substituted salicylaldehydes: Characterization and biological profile. *J. Inorg. Biochem.* **2023**, *242*, 112161. [[CrossRef](#)]
33. Zianna, A.; Vradi, E.; Hatzidimitriou, A.G.; Kalogiannis, S.; Psomas, G. Zinc(II) complexes of 3-bromo-5-chloro-salicylaldehyde: Characterization and biological activity. *Dalton Trans.* **2022**, *51*, 17629–17641. [[CrossRef](#)] [[PubMed](#)]
34. Gkritzali, M.; Georgila, M.; Hatzidimitriou, A.G.; Kalogiannis, S.; Psomas, G. Neutral and cationic nickel(II) complexes with substituted salicylaldehydes: Characterization, antibacterial activity, and interaction with biomacromolecules. *J. Inorg. Biochem.* **2023**, *247*, 112339. [[CrossRef](#)]
35. Selakovic, S.; Rodic, M.V.; Novakovic, I.; Matic, I.Z.; Stanojkovic, T.; Pirkovic, A.; Zivkovic, L.; Spremo-Potparevic, B.; Milcic, M.; Medakovic, V.; et al. Cu(II) complexes with a salicylaldehyde derivative and α -diimines as co-ligands: Synthesis, characterization, biological activity. Experimental and theoretical approach. *Dalton Trans.* **2024**, *53*, 2770–2788. [[CrossRef](#)] [[PubMed](#)]
36. Zianna, A.; Geromichalos, G.D.; Hatzidimitriou, A.G.; Coutouli-Argyropoulou, E.; Lalia-Kantouri, M.; Psomas, G. Palladium(II) complexes with salicylaldehyde ligands: Synthesis, characterization, structure, in vitro and in silico study of the interaction with calf-thymus DNA and albumins. *J. Inorg. Biochem.* **2019**, *194*, 85–96. [[CrossRef](#)]
37. Zianna, A.; Psomas, G.; Hatzidimitriou, A.; Lalia-Kantouri, M. Copper(II) complexes of salicylaldehydes and 2-hydroxyphenones: Synthesis, structure, thermal decomposition study and interaction with calf-thymus DNA and albumins. *RSC Adv.* **2015**, *5*, 37495–37511. [[CrossRef](#)]

38. Zianna, A.; Geromichalos, G.; Psoma, E.; Kalogiannis, S.; Hatzidimitriou, A.G.; Psomas, G. Structure and in vitro and in silico biological activity of zinc(II) complexes with 3,5-dichloro-salicylaldehyde. *J. Inorg. Biochem.* **2022**, *229*, 111727. [[CrossRef](#)]
39. Zianna, A.; Geromichalou, E.; Geromichalos, G.; Fiotaki, A.M.; Hatzidimitriou, A.G.; Kalogiannis, S.; Psomas, G. Zinc(II) complexes of 3,5-dibromo-salicylaldehyde and α -diimines: Synthesis, characterization and in vitro and in silico biological profile. *J. Inorg. Biochem.* **2022**, *226*, 111659. [[CrossRef](#)] [[PubMed](#)]
40. Vitomirov, T.; Dimiza, F.; Matic, I.Z.; Stanojkovic, T.; Pirkovic, A.; Zivkovic, L.; Spremo-Potparevic, B.; Novakovic, I.; Anđelkovic, K.; Milcic, M.; et al. Copper(II) complexes with 4-(diethylamino)salicylaldehyde and α -diimines: Anticancer, antioxidant, antigenotoxic effects and interaction with DNA and albumins. *J. Inorg. Biochem.* **2022**, *235*, 111942. [[CrossRef](#)]
41. Lalia-Kantouri, M.; Gdaniec, M.; Choli-Papadopoulou, T.; Badounas, A.; Papadopoulos, C.D.; Czapik, A.; Geromichalos, G.D.; Sahpazidou, D.; Tsitouroudi, F. Effect of cobalt(II) complexes with dipyriddyamine and salicylaldehydes on cultured tumor and non-tumor cells: Synthesis, crystal structure investigations and biological activity. *J. Inorg. Biochem.* **2012**, *117*, 25–34. [[CrossRef](#)]
42. Lalia-Kantouri, M.; Papadopoulos, C.D.; Hatzidimitriou, A.G.; Bakas, T.; Pachini, S. A Trinuclear Iron(III) Complex Containing the Semi-Cubane $[\text{Fe}_3(\mu_3\text{-O})_7]^+$ Core: Structural, Spectroscopic, Magnetic and Electrochemical Study. *Z. Anorg. Allg. Chem.* **2010**, *636*, 531–538. [[CrossRef](#)]
43. Anastasiadou, D.; Zianna, A.; Gdaniec, M.; Sigalas, M.P.; Coutouli-Argyropoulou, E.; Czapik, A.; Lalia-Kantouri, M. Unusual coordination mode of 3-methoxysalicylaldehyde in mononuclear zinc(II) complexes with nitrogenous bases: Synthesis, structural characterization and theoretical studies. *Polyhedron* **2015**, *87*, 275–285. [[CrossRef](#)]
44. Shool, M.T.; Rudbari, H.A.; Gil-Anton, T.; Cuevas-Vicario, J.V.; García, B.; Busto, N.; Moini, N.; Blacque, O. The effect of halogenation of salicylaldehyde on the antiproliferative activities of $\{\Delta/\Lambda\text{-}[\text{Ru}(\text{bpy})_2(\text{X},\text{Y}\text{-sal})]\text{BF}_4\}$ complexes. *Dalton Trans.* **2022**, *51*, 7658–7672. [[CrossRef](#)]
45. Mandal, A.; Jaman, M.A.; Chakraborty, I.; Chowdhury, S. Salicylaldehyde derived ligands unlocking stable oxorhenium(V) compounds: An insightful role of chloroform dimer and catalysis. *J. Mol. Struct.* **2025**, *1340*, 142552. [[CrossRef](#)]
46. Dimitrijevic, T.; Novakovic, I.; Radanovic, D.; Novakovic, S.B.; Rodic, M.V.; Andjelkovic, K.; Sumar-Ristic, M. Synthesis, spectral and structural characterization and biological activity of Cu(II) complexes with 4-(diethylamino)salicylaldehyde and α -diimines. *J. Coord. Chem.* **2020**, *73*, 702–716. [[CrossRef](#)]
47. Kuwar, A.; Tayade, K.; Keshav, K.; Sahoo, S.K.; Mayank; Singh, N. Cu^{2+} -driven metallo-supramolecular self-assembly and its application in sensing of hydroxyl ion. *Supramol. Chem.* **2018**, *30*, 52–60. [[CrossRef](#)]
48. Zhu, X.W. Synthesis, Crystal Structures, and Catalytic Properties of Dioxomolybdenum(VI) Complexes Derived from 4-Chloro-2- $\{[4\text{-Diethylamino-2-Hydroxybenzylidene}]\text{amino}\}$ phenol. *Russ. J. Coord. Chem.* **2019**, *45*, 532–538. [[CrossRef](#)]
49. Abedin, N.; Alshehri, A.H.A.; Almughrbi, A.M.A.; Moore, O.; Alyza, S.; Rusbridge, E.K.; Masood, N.; Egbowon, B.F.; Hargreaves, A.J.; Dafnis-Calas, F.; et al. Expanding the family of tetrahalide iron complexes: Synthesis, structure and biological applications. *Polyhedron* **2020**, *190*, 114755. [[CrossRef](#)]
50. Patel, K.N.; Patel, N.H.; Patel, K.M.; Patel, M.N.; Kothari, I.L. Synthesis, Characterization and Antimicrobial Activities of Some Transition Metal Complexes Containing Two Bidentate (O-O) Monobasic Hydroxy Aldehydes and 2,2'-Bipyridylamine. *Synth. React. Inorg. Met.-Org. Chem.* **2000**, *30*, 829–841. [[CrossRef](#)]
51. Geary, W.J. The use of conductivity measurements in organic solvents for the characterisation of coordination compounds. *Coord. Chem. Rev.* **1971**, *7*, 81–122. [[CrossRef](#)]
52. Chun, H.; Verani, C.N.; Chaudhuri, P.; Bothe, E.; Bill, E.; Weyhermüller, T.; Wieghardt, K. Molecular and electronic structure of octahedral o-aminophenolato and o-iminobenzosemiquinonato complexes of V(V), Cr(III), Fe(III), and Co(III). Experimental determination of oxidation levels of ligands and metal ions. *Inorg. Chem.* **2001**, *40*, 4157–4166. [[CrossRef](#)] [[PubMed](#)]
53. Lalia-Kantouri, M.; Dimitriadis, T.; Papadopoulos, C.D.; Gdaniec, M.; Czapik, A.; Hatzidimitriou, A.G. Synthesis and structural characterization of iron(III) complexes with 2-hydroxyphenones. *Z. Anorg. Allg. Chem.* **2009**, *635*, 2185–2190. [[CrossRef](#)]
54. Hamlaoui, M.; Hamlaoui, I.; Damous, M.; Belhocine, Y.; Sbei, N.; Ali, F.A.M.; Alghamdi, M.A.; Talab, S.; Rahali, S.; Merazig, H. Synthesis of Two Novel Copper (II) Complexes as Potential Inhibitors of HIV-1 Protease Enzyme: Experimental and Theoretical Investigations. *Crystals* **2022**, *12*, 1066. [[CrossRef](#)]
55. Shaikh, N.A.; Rathod, S.N.; Bhat, S.S.; Naveen, S.; Shaikh, S.; Mahesha; Revankar, V.K.; Lokanath, N.K. Synthesis, Structural Characterization and Hirshfeld Surface Analysis of Mixed Ligand Copper(II) Complex. *Chem. Data Collect.* **2020**, *28*, 100374. [[CrossRef](#)]
56. Asgharpour, Z.; Farzaneh, F.; Abbasi, A. Synthesis, characterization and immobilization of a new cobalt(II) complex on modified magnetic nanoparticles as catalyst for epoxidation of alkenes and oxidation of activated alkanes. *RSC Adv.* **2016**, *6*, 95729–95739. [[CrossRef](#)]
57. Hazra, S.; Majumdar, D.; Frontera, A.; Roy, S.; Gassoumi, B.; Ghalla, H.; Dalai, S. On the Significant Importance of $\text{Hg} \cdots \text{Cl}$ Spodium Bonding/ σ/π -Hole/Noncovalent Interactions and Nanoelectronic/Conductivity Applications in Mercury Complexes: Insights from DFT Spectrum. *Cryst. Growth Des.* **2024**, *24*, 7246–7261. [[CrossRef](#)]

58. Wang, Y.Z.; Wang, P.; Li, C.; Su, Y.Q. Synthesis, Crystal Structure and Sulfoxidation of an Iron(III) Complex Derived From 3-Methoxysalicylaldehyde, Synthesis and Reactivity in Inorganic. *Met.-Org. Nano-Met. Chem.* **2016**, *46*, 868–871. [CrossRef]
59. Nesterova, O.V.; Vassilyeva, O.Y.; Skelton, B.W.; Bienko, A.; Pompeiro, A.J.L.; Nesterov, D.S. A novel o-vanillin Fe(III) complex catalytically active in C-H oxidation: Exploring the magnetic exchange interactions and spectroscopic properties with different DFT functionals. *Dalton Trans.* **2021**, *50*, 14782–14796. [CrossRef]
60. Vassilyeva, O.Y.; Buvaylo, E.A.; Kokozay, V.N.; Skelton, B.W.; Sobolev, A.N.; Bienko, A.; Ozarowski, A. Ferro- vs. antiferromagnetic exchange between two Ni(II) ions in a series of Schiff base heterometallic complexes: What makes the difference? *Dalton Trans.* **2021**, *50*, 2841–2853. [CrossRef]
61. Costes, J.P.; Dahan, F.; Vendier, L.; Shova, S.; Lorusso, G.; Evangelisti, M. NiII-LnIII complexes with o-vanillin as the main ligand: Syntheses, structures, magnetic and magnetocaloric properties. *Dalton Trans.* **2018**, *47*, 1106–1116. [CrossRef]
62. Vassilyeva, O.Y.; Nesterova, O.V.; Bieńko, A.; Komarnicka, U.K.; Buvaylo, E.A.; Vasylieva, S.M.; Skelton, B.W.; Nesterov, D.S. Heterometallic CuCd and CuZn complexes with o-vanillin and its Schiff-base derivative: Slow magnetic relaxation and catalytic activity associated with CuII centres. *Dalton Trans.* **2025**, *54*, 6117–6132. [CrossRef] [PubMed]
63. Mondal, A.; Mondal, M.; Das, R.; Ghosh, M.; Bhowmik, A.; Biswas, B.; Banerjee, P. A homobimetallic nickel(II) complex for discriminative chromogenic recognition of aqueous cyanide and silver(I) from medicinal products: Role of end-on thiocyanate bridging. *Inorganica Chim. Acta* **2024**, *573*, 122322. [CrossRef]
64. Zhang, S.H.; Li, N.; Ge, C.M.; Feng, C.; Ma, L.F. Structures and magnetism of $\{Ni_2Na_2\}$, $\{Ni_4\}$ and $\{Ni_6^{II}Ni^{III}\}$ 2-hydroxy-3-alkoxy-benzaldehyde clusters. *Dalton Trans.* **2011**, *40*, 3000–3007. [CrossRef] [PubMed]
65. Costes, J.P.; Vendier, L.; Wernsdorfer, W. Structural and magnetic studies of original tetranuclear CoII-LnIII complexes (LnIII = Gd, Tb, Y). *Dalton Trans.* **2011**, *40*, 1700–1706. [CrossRef]
66. Biswas, R.; Drew, M.G.B.; Ghosh, A. Synthesis and crystal structure of a novel octa-aqua bridged star-shaped Ni₄K complex. *Inorg. Chem. Commun.* **2012**, *24*, 1–3. [CrossRef]
67. Arion, V.B.; Kravtsov, V.C.; Gradinaru, J.I.; Simonov, Y.A.; Gerbeleu, N.V.; Lipkowski, J.; Wignacourt, J.P.; Vezin, H.; Mentre, O. Potassium-controlled synthesis of heterotopic macrocycles based on isothiosemicarbazide. *Inorganica Chim. Acta* **2002**, *328*, 123–133. [CrossRef]
68. Diop, M.; Sarr, M.; Diop, A.; Thiam, I.E.; Barry, A.H.; Gaye, M.; Alvarez, N.; Ellena, J. Nickel(II)-complex ligand as host for Potassium ion guest. Spectroscopic characterization and X-ray structure determination. *IOSR J. Appl. Chem.* **2019**, *12*, 18–24. Available online: <https://www.iosrjournals.org/iosr-jac/papers/vol12-issue1/series-1/E1201011824.pdf> (accessed on 22 January 2019).
69. Jeffery, J.C.; Jelliss, P.A.; Rudd, G.E.A.; Sakanishi, S.; Stone, F.G.A.; Whitehead, J. Some di- and tri-metal complexes derived from the synthon $[Ru(CO)_2(THF)(\eta^5-7,8-C_2B_9H_{11})]$. *J. Organomet. Chem.* **1999**, *582*, 90–99. [CrossRef]
70. Wang, Q.; Manzano, R.A.; Tinnermann, H.; Sung, S.; Leforestier, B.; Krämer, T.; Young, R.D. Access to and Reactivity of Fe⁰, Fe–I, FeI, and FeII PCarbeneP Pincer Complexes. *Angew. Chem. Int. Ed.* **2021**, *60*, 18168–18177. [CrossRef]
71. Reinfandt, N.; Michenfelder, N.; Schoo, C.; Yadav, R.; Reichl, S.; Konchenko, S.N.; Unterreiner, A.N.; Scheer, M.; Roesky, P.W. d/f-Polynictides Derived by Non-Classical Ln²⁺ Compounds: Synthesis, Small Molecule Activation and Optical Properties. *Chemistry* **2021**, *27*, 7862–7871. [CrossRef]
72. Zeglis, B.M.; Pierre, V.C.; Barton, J.K.; Pierre, V.C. Metallo-intercalators and metallo-insertors. *Chem. Commun.* **2007**, *44*, 4565–4579. [CrossRef] [PubMed]
73. Pages, B.J.; Ang, D.L.; Wright, E.P.; Aldrich-Wright, J.R. Metal complex interactions with DNA. *Dalton Trans.* **2015**, *44*, 3505–3526. [CrossRef]
74. Pyle, A.M.; Rehmann, J.P.; Meshoyrer, R.; Kumar, C.V.; Turro, N.J.; Barton, J.K. Mixed-ligand complexes of ruthenium(II): Factors governing binding to DNA. *J. Am. Chem. Soc.* **2002**, *111*, 3051–3058. [CrossRef]
75. Wolfe, A.; Shimer, G.H.; Meehan, T. Polycyclic Aromatic Hydrocarbons Physically Intercalate into Duplex Regions of Denatured DNA. *Biochemistry* **1987**, *26*, 6392–6396. [CrossRef] [PubMed]
76. Dimitrakopoulou, A.; Dendrinou-Samara, C.; Pantazaki, A.A.; Alexiou, M.; Nordlander, E.; Kessissoglou, D.P. Synthesis, structure and interactions with DNA of novel tetranuclear, $[Mn_4(II/II/II/IV)]$ mixed valence complexes. *J. Inorg. Biochem.* **2008**, *102*, 618–628. [CrossRef]
77. Pizarro, A.M.; Sadler, P.J. Unusual DNA binding modes for metal anticancer complexes. *Biochimie* **2009**, *91*, 1198–1211. [CrossRef]
78. Lakowicz, J.R. *Principles of Fluorescence Spectroscopy*; Springer: Berlin/Heidelberg, Germany, 2006. Available online: <https://link.springer.com/book/10.1007/978-0-387-46312-4> (accessed on 12 February 2023).
79. Heller, D.P.; Greenstock, C.L. Fluorescence lifetime analysis of DNA intercalated ethidium bromide and quenching by free dye. *Biophys. Chem.* **1994**, *50*, 305–312. [CrossRef]

80. Ross, P.D.; Subramanian, S. Thermodynamics of Protein Association Reactions: Forces Contributing to Stability. *Biochemistry* **1981**, *20*, 3096–3102. [[CrossRef](#)]
81. Rodrigues, B.M.; Victória, H.F.V.; Leite, G.; Krambrock, K.; Chaves, O.A.; de Oliveira, D.F.; de Q, R.; de Boni, L.; Costa, L.A.S.; Iglesias, B.A. Photophysical, photobiological, and biomolecule-binding properties of new tri-cationic meso-tri(2-thienyl)corroles with Pt(II) and Pd(II) polypyridyl derivatives. *J. Inorg. Biochem.* **2023**, *242*, 112149. [[CrossRef](#)]
82. Sakthikumar, K.; Krause, R.W.M.; Isamura, B.K.; Raja, J.D.; Athimoolam, S. Spectro-electrochemical, fluorometric and biothermodynamic evaluation of pharmacologically active morpholine scaffold single crystal ligand and its metal(II) complexes: A comparative study on in-vitro and in-silico screening towards DNA/BSA/SARS-CoV-19. *J. Inorg. Biochem.* **2022**, *236*, 111953. [[CrossRef](#)]
83. Sakthikumar, K.; Solomon, R.V.; Raja, J.D. Spectro-electrochemical assessments of DNA/BSA interactions, cytotoxicity, radical scavenging and pharmacological implications of biosensitive and biologically active morpholine-based metal(II) complexes: A combined experimental and computational investigation. *RSC Adv.* **2019**, *9*, 14220–14241. [[CrossRef](#)] [[PubMed](#)]
84. Kashanian, S.; Askari, S.; Ahmadi, F.; Omidfar, K.; Ghobadi, S.; Tarighat, F.A. In Vitro Study of DNA Interaction with Clodinafop-Propargyl Herbicide. *DNA Cell Biol.* **2008**, *27*, 581–586. [[CrossRef](#)]
85. Papastergiou, A.; Perontsis, S.; Gritzapis, P.; Koumbis, A.E.; Koffa, M.; Psomas, G.; Fylaktakidou, K.C. Evaluation of O-alkyl and aryl sulfonyl aromatic and heteroaromatic amidoximes as novel potent DNA photo-cleavers. *Photochem. Photobiol. Sci.* **2016**, *15*, 351–360. [[CrossRef](#)]
86. Tarushi, A.; Lafazanis, K.; Kljun, J.; Turel, I.; Pantazaki, A.A.; Psomas, G.; Kessissoglou, D.P. First- and second-generation quinolone antibacterial drugs interacting with zinc(II): Structure and biological perspectives. *J. Inorg. Biochem.* **2013**, *121*, 53–65. [[CrossRef](#)] [[PubMed](#)]
87. Tarushi, A.; Kljun, J.; Turel, I.; Pantazaki, A.A.; Psomas, G.; Kessissoglou, D.P. Zinc(II) complexes with the quinolone antibacterial drug flumequine: Structure, DNA- and albumin-binding. *New J. Chem.* **2013**, *37*, 342–355. [[CrossRef](#)]
88. Stella, L.; Capodilupo, A.L.; Bietti, M. A reassessment of the association between azulene and [60]fullerene. Possible pitfalls in the determination of binding constants through fluorescence spectroscopy. *Chem. Commun.* **2008**, 4744–4746. [[CrossRef](#)]
89. Laitinen, O.H.; Hytönen, V.P.; Nordlund, H.R.; Kulomaa, M.S. Genetically engineered avidins and streptavidins. *Cell. Mol. Life Sci.* **2006**, *63*, 2992–3017. [[CrossRef](#)]
90. Lazou, M.; Tarushi, A.; Gritzapis, P.; Psomas, G. Transition metal complexes with a novel guanine-based (E)-2-(2-(pyridin-2-ylmethylene)hydrazinyl)quinazolin-4(3H)-one: Synthesis, characterization, interaction with DNA and albumins and antioxidant activity. *J. Inorg. Biochem.* **2020**, *206*, 111019. [[CrossRef](#)]
91. Cini, R.; Giorgi, G.; Cinquantini, A.; Rossi, C.; Sabat, M. Metal Complexes of the Antiinflammatory Drug Piroxicam. *Inorg. Chem.* **1990**, *29*, 5197–5200. [[CrossRef](#)]
92. Marchi, R.C.; Campos, I.A.S.; Santana, V.T.; Carlos, R.M. Chemical implications and considerations on techniques used to assess the in vitro antioxidant activity of coordination compounds. *Coord. Chem. Rev.* **2022**, *451*, 2142752. [[CrossRef](#)]
93. Ali, B.M.; Boothapandi, M.; Nasar, A.S.S. Nitric oxide, DPPH and hydrogen peroxide radical scavenging activity of TEMPO terminated polyurethane dendrimers: Data supporting antioxidant activity of radical dendrimers. *Data Brief* **2020**, *28*, 104972. [[CrossRef](#)] [[PubMed](#)]
94. Dairi, S.; Carbonneau, M.A.; Galeano-Diaz, T.; Remini, H.; Dahmoune, F.; Aoun, O.; Belbahi, A.; Lauret, C.; Cristol, J.P.; Madani, K. Antioxidant effects of extra virgin olive oil enriched by myrtle phenolic extracts on iron-mediated lipid peroxidation under intestinal conditions model. *Food Chem.* **2017**, *237*, 297–304. [[CrossRef](#)]
95. Kontogiorgis, C.; Hadjipavlou-Litina, D. Biological evaluation of several coumarin derivatives designed as possible anti-inflammatory/antioxidant agents. *J. Enzym. Inhib. Med. Chem.* **2003**, *18*, 63–69. [[CrossRef](#)] [[PubMed](#)]
96. Wettasinghe, M.; Shahidi, F. Scavenging of reactive-oxygen species and DPPH free radicals by extracts of borage and evening primrose meals. *Food Chem.* **2000**, *70*, 17–26. [[CrossRef](#)]
97. Marmur, J. A procedure for the isolation of deoxyribonucleic acid from micro-organisms. *J. Mol. Biol.* **1961**, *3*, 208–218. [[CrossRef](#)]
98. Reichmann, M.E.; Rice, S.A.; Thomas, C.A.; Doty, P. A Further Examination of the Molecular Weight and Size of Desoxyribose Nucleic Acid. *J. Am. Chem. Soc.* **1954**, *76*, 3047–3053. [[CrossRef](#)]
99. Bruker Analytical X-ray Systems, Inc. *Apex2, Version 2 User Manual, M86-E01078*; Bruker Analytical X-ray Systems, Inc.: Madison, WI, USA, 2006.
100. Siemens Industrial Automation, Inc. *SADABS: Area-Detector Absorption Correction*; Siemens Industrial Automation, Inc.: Plano, TX, USA, 1996.
101. Palatinus, L.; Chapuis, G. SUPERFLIP—a computer program for the solution of crystal structures by charge flipping in arbitrary dimensions. *J. Appl. Crystallogr.* **2007**, *40*, 786–790. [[CrossRef](#)]
102. Betteridge, P.W.; Carruthers, J.R.; Cooper, R.I.; Prout, K.; Watkin, D.J. CRYSTALS version 12: Software for guided crystal structure analysis. *J. Appl. Crystallogr.* **2003**, *36*, 1487. [[CrossRef](#)]

103. Wang, Y.-Q.; Zhang, H.-M.; Zhang, G.-C.; Tao, W.-H.; Tang, S.-H. Interaction of the flavonoid hesperidin with bovine serum albumin: A fluorescence quenching study. *J. Lumin.* **2007**, *126*, 211–218. [[CrossRef](#)]
104. Ruch, R.J.; Cheng, S.J.; Klaunig, J.E. Prevention of cytotoxicity and inhibition of intercellular communication by antioxidant catechins isolated from Chinese green tea. *Carcinogenesis* **1989**, *10*, 1003–1008. [[CrossRef](#)]
105. de Meulenaer, J.; Tompa, H. The absorption correction in crystal structure analysis. *Acta Crystallogr.* **1965**, *19*, 1014–1018. [[CrossRef](#)]

Disclaimer/Publisher’s Note: The statements, opinions and data contained in all publications are solely those of the individual author(s) and contributor(s) and not of MDPI and/or the editor(s). MDPI and/or the editor(s) disclaim responsibility for any injury to people or property resulting from any ideas, methods, instructions or products referred to in the content.